

Proposal for the J-PARC 30-GeV Proton Synchrotron

## Investigation of fundamental properties of the $\bar{K}NN$ state

H. Asano, K. Itahashi, M. Iwasaki, Y. Ma, R. Murayama, H. Outa, F. Sakuma,  
T. Yamaga\*

*RIKEN Cluster for Pioneering Research, RIKEN, Saitama, 351-0198, Japan*

K. Inoue, S. Kawasaki, H. Noumi, K. Shirotori  
*Research Center for Nuclear Physics (RCNP), Osaka University, Osaka, 567-0047,  
Japan*

H. Ohnishi, Y. Sada, C. Yoshida  
*Research Center for Electron Photon Science (ELPH), Tohoku University, Sendai,  
982-0826, Japan*

T. Hashimoto, K. Tanida  
*Japan Atomic Energy Agency (JAEA), Ibaraki 319-1195, Japan*

M. Iio, S. Ishimoto, K. Ozawa, S. Suzuki  
*High Energy Accelerator Research Organization (KEK), Ibaraki, 305-0801, Japan*

T. Akaishi  
*Department of Physics, Osaka University, Osaka, 560-0043, Japan*

T. Nagae  
*Department of Physics, Kyoto University, Kyoto, 606-8502, Japan*

H. Fujioka, D. Jido  
*Department of Physics, Tokyo Institute of Technology, Tokyo, 152-8551, Japan*

M. Bazzi, A. Clozza, C. Curceanu, C. Guaraldo, M. Iliescu, M. Miliucci, A. Scordo,  
D. Sirghi, F. Sirghi  
*Laboratori Nazionali di Frascati dell' INFN, I-00044 Frascati, Italy*

J. Marton, H. Shi, M. Tuechler, E. Widmann, J. Zmeskal  
*Stefan-Meyer-Institut für subatomare Physik, A-1090 Vienna, Austria*

T. Sekihara  
*Graduate School of Life and Environmental Science, Kyoto Prefectural University,*

---

\*Spokesperson, E-mail: takumi.yamaga@riken.jp

*Kyoto, 606-8522, Japan*

### **Abstract**

The  $I_z = +1/2$   $\bar{K}NN$  state, the “ $K^-pp$ ” bound state, exchanging  $\sim$  on-shell  $\bar{K}$  between two nucleons, has been exhibited by the J-PARC E15 experiment. A momentum transfer analysis based on a PWIA suggests that the size of the “ $K^-pp$ ” could be surprisingly small as the two protons being overlapping with each other. If the internal structure and/or implied size can be confirmed, a new research field to access a high-density and cold-temperature regime in the QCD phase diagram will be opened. Towards the prospect, fundamental properties of the  $\bar{K}NN$  system should be examined more comprehensive manner, thus we propose a new experiment on  $\bar{K}NN$ , especially focusing on the spin and parity of the state. We will measure the energy of  $I_z = -1/2$   $\bar{K}NN$  state, the “ $\bar{K}^0nn$ ” bound state, and spin-spin correlation ( $\alpha_{\Lambda p}$ ) of  $\Lambda p$  of  $I_z = +1/2$   $\bar{K}NN$ . Both “ $\bar{K}^0nn$ ” and “ $K^-pp$ ” will be produced and measured exclusively by the  $K^- + {}^3\text{He} \rightarrow \Lambda pn$  reaction. With 8 weeks beam-time, we will confirm the existence of the “ $\bar{K}^0nn$ ” for the first time, and determine the spin and parity of the  $\bar{K}NN$ . In parallel to the experimental study, we wish to establish the theoretical framework to extend the physics program to be opened in future.

## Summary of the proposed experiment

<b>Beam-line:</b>	K1.8BR
<b>Primary beam:</b>	30 GeV, 90kW (5.2 s spill interval)
<b>Secondary beam:</b>	1.0 GeV/ $c$ $K^-$
<b>Beam intensity:</b>	$3.2 \times 10^5$ on target per pulse
<b>Reaction:</b>	in-flight ( $K^-$ , $N$ )
<b>Detectors:</b>	improved K1.8BR beam-line spectrometer, and new cylindrical detector system
<b>Target:</b>	Liquid $^3\text{He}$
<b>Beam-time:</b>	8 weeks for the physics run (648 kW · week)

# 1 Physics motivation

We propose a new experiment to investigate fundamental properties of the  $\bar{K}NN$  bound state, the simplest system among the kaonic nuclei. Especially, we are going to determine the spin and parity  $J^P$  that defines the internal structure of  $\bar{K}NN$  ( $I_z = +1/2$ ) and observe energy difference of its isospin doublet partner ( $I_z = -1/2$ ). Through the experiment, we can establish the basis to understand  $\bar{K}N$  interaction in the energy region below the mass threshold.

The existence of kaonic nuclear bound states is natural extension of the Dalitz's prediction, *i.e.*,  $\Lambda(1405)$  can be an atom-like  $\bar{K}N$  hadronic bound state due to the strong attractive interaction in the isospin  $I_{\bar{K}N} = 0$  channel, rather than three quark baryon [1, 2]. This interpretation is widely accepted, and as a result, it leads many theoretical predictions of variety of kaonic nuclear bound states [3, 4, 5, 6, 7, 8, 9, 10, 11, 12, 13, 14, 15, 16, 17, 18], in which  $\bar{K}$  would form molecule-like nuclear states together with multi-nucleons by exchanging  $\bar{K}$ . This is peculiar nuclear system, in which  $\sim$  on-shell  $\bar{K}$ -meson coexists with nucleons as a constituent of the system. In normal nuclei, the simplest picture of the source of the binding energy is the virtual pion exchange whose energy budget is close to its mass  $\sim m_\pi$  ( $\approx 140$  MeV/ $c^2$ ), and the virtuality of the exchanging  $\pi$ -meson is quite high. On the contrary,  $\bar{K}$ -meson in nuclear system would be very close to the on-shell mass, so the energy budget of the  $\bar{K}$ -meson exchange ( $m_{K^-} + m_p - m_{\Lambda(1405)} \approx 10 \sim 25$  MeV/ $c^2$ ) is much smaller than the  $\pi$ -meson exchange. This will help to form deep binding energy in kaonic nuclei together with the strong attraction of  $\bar{K}N$  interaction in  $I_{\bar{K}N} = 0$  channel. In addition, pion exchange is forbidden in the first order due to the isospin rule. On the other hand, there are short-range  $NN$  repulsion in the system, therefore kaonic nuclei would have specific spatial configuration of elements, like it is the case of chemical molecule.

## 1.1 Previous experiment, J-PARC E15

Before describing detailed necessity of the proposed experiment, we shortly review the result of the J-PARC E15 experiment; observation of “ $K^-pp$ ” (symbolical notation of  $\bar{K}NN$   $I_z = +1/2$ ), to make it clear what we have known about the  $\bar{K}NN$  system. We carried out the E15 experiment to search for the “ $K^-pp$ ”, using the in-flight  $K^- + {}^3\text{He}$  reaction with an exclusive analysis of the  $\Lambda pn$  final state [19, 20, 21], where the  $\Lambda p$  is the simplest decay channel of the “ $K^-pp$ ” to be detected easily. A two-dimensional distribution of the  $\Lambda p$  invariant-mass and the momentum transfer to the  $\Lambda p$  system were obtained in the experiment as shown in Fig. 1-(a). The “ $K^-pp$ ” signal is clearly observed as a vertical event-concentration at the  $\Lambda p$  invariant-mass below the “ $K^-pp$ ” mass-threshold in the lower momentum transfer region. In the figure, the decomposition of reaction processes is given in each projection, and the “ $K^-pp$ ” formation process is shown in red.

On the other hand, in the mass-region larger than the “ $K^-pp$ ” mass-threshold, there are two additional events-concentrations at momentum transfer regions around

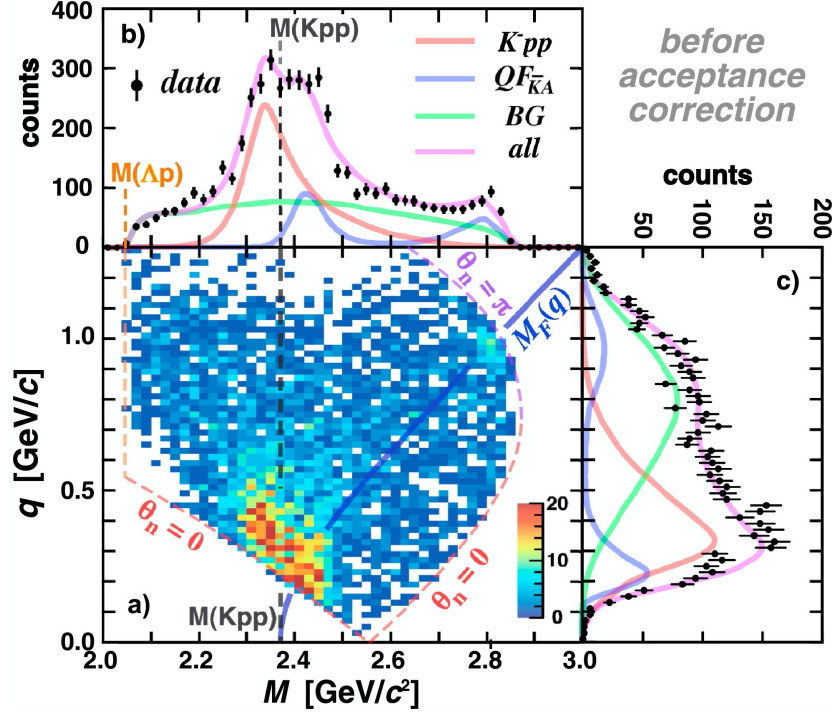


Figure 1: (a) Two dimensional event distribution on the plane of the  $\Lambda p$  invariant-mass ( $m_{\Lambda p}$ ) and momentum transfer to the  $\Lambda p$  system ( $q_{\Lambda p}$ ). (b) and (c) are projection spectra on  $m_{\Lambda p}$  and  $q_{\Lambda p}$  axes, respectively. The colored lines in (b) and (c) are the fitting result. The figure was taken from Ref. [20]. We plotted the figure in a count basis without applying acceptance correction, to make it easy to see the statistical uncertainty, and to compare simulated spectra given in this proposal.

0.2 and 1.0 GeV/c. As shown in the figure, these events-concentrations exist along the blue kinematical line (denoted as  $M_F(q)$ ), where  $\Lambda N$ -pair should locate if the final interaction is the quasi-free  $\bar{K}$  ( $\sim$  on-shell  $\bar{K}$  having momentum  $q$ ) absorption by spectator ( $\sim$  at-rest) two nucleons  $NN$ . Thus, we interpreted that both event-concentrations are produced by quasi-free kaon absorption ( $QF_{\bar{K}-abs}$ ) process, originated by a  $K^- N \rightarrow \bar{K} n$  reaction followed by a  $\bar{K}$ -absorption by the residual two nucleons.

In addition, there is a broad distribution covering whole kinematically allowed region (shown by the green line in each projection). The most probable and natural interpretation is an alternative charge reaction of the  $QF_{\bar{K}-abs}$  process, *i.e.*,  $K^- p \rightarrow K^- p$  followed by  $K^- pn \rightarrow \Lambda n$ , so that no clear event correlation is expected when  $\Lambda p$ -pair (misconceiving pair) is analyzed. As a result, a broad distribution is formed because of the misconceiving analysis.

We wish to stress that the  $K^- + {}^3\text{He} \rightarrow Y N_1 N_2$  events distribution can be described very nicely with an unique physics process summarized as;  $K^- N \rightarrow \bar{K} N_j$  followed by  $\bar{K} NN \rightarrow \Lambda N_k$  ( $j, k = 1$  or  $2$ , exclusively), in which intermediate  $\bar{K}$  is  $\sim$  on-shell and

the successive reaction happens within the time-interval allowed by the uncertainty principle. If the invariant-mass  $\text{IM}(\bar{K}NN)$  is below the mass threshold,  $\bar{K}NN$  bound state is dominantly formed as a quantum state, while  $\text{QF}_{\bar{K}\text{-abs}}$  happens in a competing manner, if  $\text{IM}(\bar{K}NN)$  is above that. Consequently, strong events-concentration is formed in  $\text{IM}(\Lambda N_k)$  analysis, over the broad event distribution caused by the misconceiving  $\text{IM}(\Lambda N_j)$  analysis.

The unique reaction scheme (or dominance of that) is the biggest advantage of E15's exclusive  $\Lambda pn$  reaction channel, in which the presence of  $\sim$  on-shell  $\bar{K}$  in the intermediate state is secured. No other complicated reaction channels are required to describe the experimental data, and the suppression of those backgrounds is insured because of the minimal number of baryons in the final state,  $\Lambda pn$ . On the other hand, if it is explored with stable particles,  $\bar{s}s$ -quark pair production is required to access the kaonic nuclear bound state. This yields severe background coming from direct  $K^+\Lambda$  (or  $K^0\Lambda$ ) production without forming  $\bar{K}$ -meson in the reaction channel, that one cannot discriminate from the signal [22, 23]. This channel has an advantage also to  $K^-$  absorption at-rest [24], because we are free from multi-nucleon absorption processes, that forms severe background overlapping with formation signal in at-rest experiment.

In E15, we fitted the 2D distribution based on formula given by a PWIA calculation with harmonic oscillator wave-function for " $K^-pp$ ") to examine basic informations of the " $K^-pp$ ". The binding energy and decay width of the " $K^-pp$ " were found to be  $B.E. = 42 \pm 3(\text{stat.})_{-4}^{+3}(\text{syst.})$  MeV and  $\Gamma = 100 \pm 7(\text{stat.})_{-9}^{+19}(\text{syst.})$  MeV, respectively. The  $S$ -wave Gaussian form factor of the " $K^-pp$ " was obtained to be  $383 \pm 11(\text{stat.})_{-1}^{+4}(\text{syst.})$  MeV/ $c$ .

The obtained binding energy is consistent with theoretical predictions based on the phenomenological  $\bar{K}N$  interaction model [25, 5, 11, 14, 9]. On the other hand, the obtained decay width is larger than that of  $\Lambda(1405) \rightarrow \Sigma\pi$ ,  $\Gamma \sim 50$  MeV (100%), which is consistent with the theoretical understanding that the major  $\bar{K}NN$  decay channel occurs through  $I_{\bar{K}N} = 0$  pole (namely,  $\Lambda(1405)$ ), hence  $\bar{K}NN$  should be unstable than  $\Lambda(1405)$ . In fact, none of these calculations have considered non-mesonic decay branches, while channels are widely open. We need to wait for the theoretical progress to compare with the data, which exhibits non-mesonic decay partial width is comparable. Finally, obtained large form factor parameter implies that the spatial size of the " $K^-pp$ " is  $\sim 0.6$  fm. This size is surprisingly small in a comparison with the nucleon mean distance in nuclei,  $\sim 0.7$  fm. This suggests that two nucleons in the  $\bar{K}NN$  would be overlapping with each other by the strong attraction of  $\bar{K}$ -meson.

There are still several missing informations need to be clarified. In the E15 experiment, cross-section information is evaluated via the  $\Lambda p$  decay channel, so it is derived only partially. There are several other possible decay channels, *i.e.*,  $\Sigma N$  and  $\pi\Sigma N$ . The branching ratio to these channels will give us additional information to deduce the internal structure of the  $\bar{K}NN$ . Figure 2 shows a reaction diagram of the  $\bar{K}NN$  production. As described, a virtual  $\bar{K}$  would be exchanged between two nucleons to form a nuclear bound state. Because the  $\Lambda(1405)$  resonance has  $\bar{K}N$  molecular structure,

the internal structure of the  $\bar{K}NN$  could be strongly related to the  $\Lambda(1405)$ , which would result large decay branch to  $\pi\Sigma N$  channel ( $\Lambda(1405) \rightarrow \pi\Sigma$  100% in vacuum). The  $\Lambda(1405)$  contribution could be also studied from the branching ratio between non-mesonic channels,  $\Lambda N$  and  $\Sigma N$ , as theoretically suggested in Ref. [26]. The key to access these channels is the sufficient neutron detection capability, that can be realized in the present proposal.

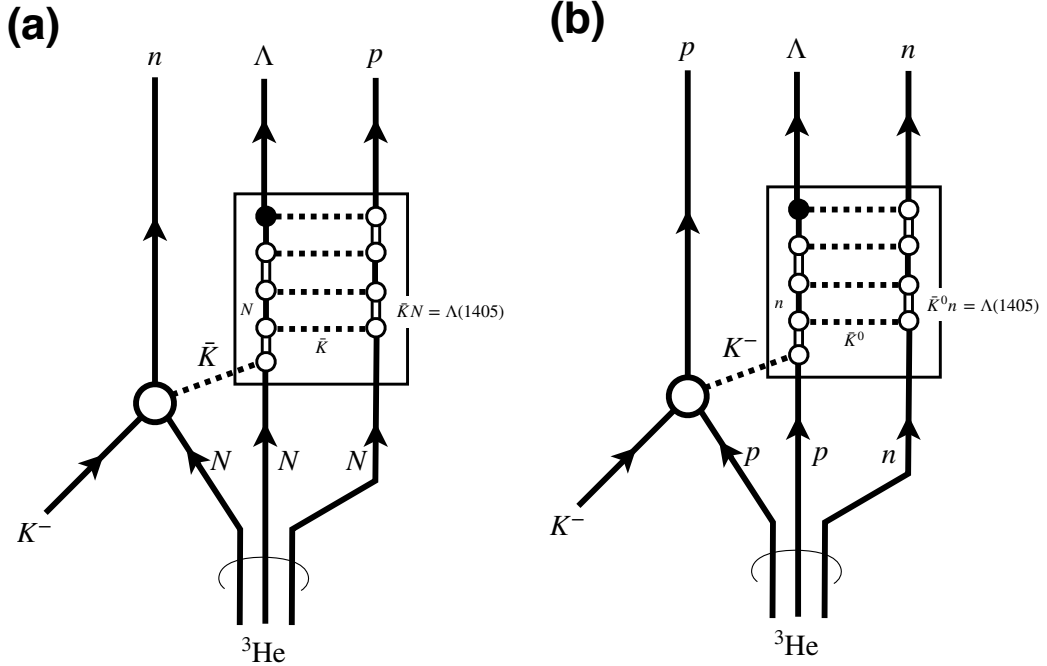


Figure 2: Reaction diagrams of (a) “ $K^-pp$ ” and (b) “ $\bar{K}^0nn$ ” production in the  $K^- + {}^3\text{He}$  reaction decaying into  $\Lambda N$  channels. In both cases, nucleon in the  ${}^3\text{He}$  is firstly knocked out through  $Y(\sim 1800)$  poles ( $\sqrt{s_{\bar{K}N}} \sim 1800$  MeV at  $p_{K^-} = 1$  GeV/ $c$  beam) and recoiled  $\bar{K}$  and two residual nucleons will form  $\bar{K}NN$ . Inside the  $\bar{K}NN$ , a virtual  $\bar{K}$  would be exchanged between  $NN$  which gives strong binding of the system where  $\bar{K}N$  part would be strongly coupled to the  $\Lambda(1405)$  resonance. At the last vertex, the virtual (largely off-shell)  $\bar{K}$  is absorbed by a nucleon to make  $\Lambda$ .

## 1.2 Specific objectives of present proposal

The missing informations and further questions arisen by E15 data motivate us to investigate the  $\bar{K}NN$  more precisely. Especially, the internal configuration and spatial size of the system are quite important to investigate how compact the  $\bar{K}NN$  is. By the present experiment, we can answer the questions and conclude that the simplest

kaonic nucleus,  $\bar{K}NN$ , is a novel nuclear system bound by kaon exchange, and forming isospin doublet whose fundamental properties are well determined.

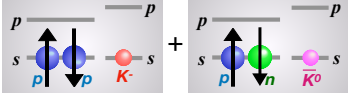
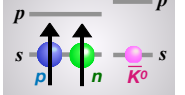
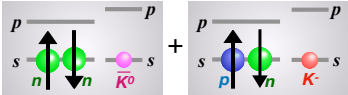
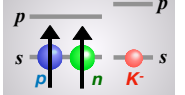
Together with J-PARC E80, we wish to open a doorway to access unexplored physical region of the QCD phase diagram at low-temperature and high-density. In that region, we are expecting rich physics, because hadron properties may change substantially as a function of chiral order parameter  $|\langle \bar{q}q \rangle|$ . We may access equation-of-state (EOS) of hadronic matter, which is essential to understand the puzzle of heavy neutron star, at present.

### 1.3 Internal configuration and $J^P$ of $\bar{K}NN$

Since good isospin symmetry is expected, the isospin doublet state  $\bar{K}NN$ ,  $I_z = -1/2$  (“ $\bar{K}^0nn$ ”) should exist, at the similar mass and having similar decay width [17]. Thus, we are going to observe “ $\bar{K}^0nn$ ” as for the final confirmation of the presence of the  $\bar{K}NN$   $I = 1/2$  doublet, and to measure the energy difference to examine isospin symmetry near the binding threshold.

Table 1 summarizes the possible internal configuration of the  $\bar{K}NN$  state with  $J^P = 0^-$  and  $1^-$ . It is naturally expected that all the particles should be in  $S$ -shell in

Table 1: Internal configuration of  $\bar{K}NN$  with  $J^P = 0^-$  and  $1^-$ .

$I (J^P)$	$\frac{1}{2} (0^-)$	$\frac{1}{2} (1^-)$
$NN$ symmetry	$(NN)_{I.sym \times S.asym} \otimes \bar{K}$	$(NN)_{I.asym \times S.sym} \otimes \bar{K}$
$I_z = +\frac{1}{2}$	 $-\frac{\sqrt{1}}{3} \left( \sqrt{2}pp\bar{K}^- + \frac{pn+np}{\sqrt{2}}\bar{K}^0 \right) \otimes \left( \frac{\uparrow\downarrow - \downarrow\uparrow}{\sqrt{2}} \right)$	 $\frac{(pn-np)}{\sqrt{2}}\bar{K}^0 \otimes \left( \uparrow\uparrow, \frac{\uparrow\downarrow + \downarrow\uparrow}{\sqrt{2}}, \downarrow\downarrow \right)$
$I_z = -\frac{1}{2}$	 $-\frac{\sqrt{1}}{3} \left( \sqrt{2}nn\bar{K}^0 + \frac{pn+np}{\sqrt{2}}\bar{K}^- \right) \otimes \left( \frac{\uparrow\downarrow - \downarrow\uparrow}{\sqrt{2}} \right)$	 $-\frac{(pn-np)}{\sqrt{2}}\bar{K}^- \otimes \left( \uparrow\uparrow, \frac{\uparrow\downarrow + \downarrow\uparrow}{\sqrt{2}}, \downarrow\downarrow \right)$
$\bar{K}N$ coupling	$\frac{ I_{\bar{K}N=0} ^2}{ I_{\bar{K}N=1} ^2} = \frac{3}{1}$	$\frac{ I_{\bar{K}N=0} ^2}{ I_{\bar{K}N=1} ^2} = \frac{1}{3}$

the ground state. Because nucleon is Fermion,  $NN$  spin should couple either symmetric or anti-symmetric manner, that defines isospin symmetry. Thus, only  $J^P = 0^-$  and  $1^-$  are reasonable candidates as for the ground state. As described in the table,  $\bar{K}N$  coupling in  $I_{\bar{K}N} = 0$  and  $I_{\bar{K}N} = 1$  channels are much different between  $J^P = 0^-$  and  $1^-$ .  $J^P = 0^-$  has larger  $I_{\bar{K}N} = 0$  component in contrast to  $1^-$ . Thus,  $J^P = 0^-$  state is naturally considered to be ground state of the  $\bar{K}NN$ , because only  $I_{\bar{K}N} = 0$  channel is

strong and very attractive. In fact,  $J^P = 1^-$  state is predicted to be unbound [27, 17], although there is contradicting calculation that it could be an excited state [28]. In the discussion above, we omitted the possibility of  $I = 3/2$ , because  $\bar{K}N$  can couple only to weak  $I_{\bar{K}N} = 1$  channel in “ $\bar{K}^0 pp$ ” and “ $K^- nn$ ” for  $J^P = 0^-$ , and these states cannot exist in  $J^P = 1^-$  due to the isospin symmetry.

$J^P$  is the most fundamental quantum number, and defines the internal configuration of  $\bar{K}NN$ , so that it must be examined and confirmed experimentally. The determination of  $J^P$  of the  $\bar{K}NN$  will lead deeper theoretical studies to understand the kaonic nuclear bound state,  $\bar{K}NN$ .

## 2 Experimental method

Let us overview the experimental method. To realize the experiment as fast as possible, we propose to perform present experiment at the K1.8BR beam-line. “ $K^-pp$ ” and “ $\bar{K}^0nn$ ” states will be produced by the in-flight  $K^- + {}^3\text{He}$  reaction and analyzed by their non-mesonic decay modes  $\Lambda p$  and  $\Lambda n$ , respectively. The produced  $\bar{K}NN$  will be identified by analyzing a two-dimensional distribution of  $\Lambda N$  invariant-mass and momentum transfer to the  $\Lambda N$  by detecting  $\Lambda$  and  $N$  (proton or neutron). We will also measure other decay modes of the  $\bar{K}NN$ , such as “ $\bar{K}^0nn$ ”  $\rightarrow \Sigma^-p$  or “ $\bar{K}^0nn$ ”  $\rightarrow \pi^\pm\Sigma^\mp n$ , to study the decay branching ratio, and to access total cross section. To realize these objectives, we need to upgrade our experimental setup to detect neutrons inside the  $\sim 4\pi$  cylindrical detector system (CDS).

For  $J^P$  determination of the  $\bar{K}NN$ , there are two possible experimental approaches. Relatively easier one is to determine the ratio of the formation cross-sections between “ $\bar{K}^0nn$ ” and “ $K^-pp$ ” ( $\sigma_{\bar{K}^0nn}/\sigma_{K^-pp}$ ). As it is described in Sec. 4 in detail,  $\sigma_{\bar{K}^0nn}/\sigma_{K^-pp}$  strongly depends on  $J^P$ , namely 0.13-0.15 for  $J^P = 0^-$  and 0.75 for  $J^P = 1^-$ . The difference of the two ratios is large and thus easy to discriminate the two. However, this approach is slightly indirect, because we need to assume good isospin symmetry in the  $\bar{K}NN$  formation ignoring detailed reaction dynamics in the decay process.

An alternative and model independent way to deduce  $J^P$  is to measure  $\Lambda$  and proton’s spin-spin correlation ( $\alpha_{\Lambda p}$ ) from the “ $K^-pp$ ”  $\rightarrow \Lambda p$  decay. In the decay, spin-parity of the initial  $K^-pp$  are conserved because it is strong interaction induced decay channel. For the  $\Lambda p$  system, total spin  $J_{\Lambda p}$  and parity  $P_{\Lambda p}$  are determined from the synthesis spin ( $S_{\Lambda p}$ ) and orbital angular momentum ( $L_{\Lambda p}$ ) as follows,

$$\begin{aligned} J_{\Lambda p} &= L_{\Lambda p} \otimes S_{\Lambda p}, \\ P_{\Lambda p} &= (-1)^{L_{\Lambda p}}. \end{aligned} \quad (1)$$

Thus, the minimum angular momentum is  $L_{\Lambda p} = 1$  to make negative parity in both cases. In  $J^P = 0^-$ ,  $S_{\Lambda p}$  must be one, so  $\Lambda p$ -pair spins shall be parallel ( $\alpha_{\Lambda p} = +1$ ). For  $J^P = 1^-$ ,  $L_{\Lambda p} = 1$  couples with  $S_{\Lambda p} = 0$  and 1 at the ratio of 1 : 2, so the  $\alpha_{\Lambda p}$  is  $+1/3$ . Therefore, we can distinguish  $J^P = 0^-$  and  $1^-$  by the  $\alpha_{\Lambda p}$  measurement.

The experimental method to measure  $\alpha_{\Lambda p}$  is as illustrated in Fig. 3. The most likely spin direction of  $\Lambda$  can be estimated from  $\Lambda \rightarrow p\pi^-$  weak-decay asymmetry ( $\alpha_- = 0.72$ ), defined by the motional direction of the decay proton (denoted as  $\vec{S}_\Lambda^o$  ( $\Lambda \rightarrow p\pi^-$ ) in Fig. 3). On the other hand, the spin direction of proton from “ $K^-pp$ ”  $\rightarrow \Lambda p$  decay can only be estimated through  $p$ -C scattering on a polarimeter via its azimuthal asymmetry ( $\langle A_{pC} \rangle \sim 0.3$ , in the present case). The estimated proton spin direction ( $\vec{S}_p^{o\perp}$ ) is the vector product of the initial proton momentum ( $\vec{p}_p^i$ ) and the final one ( $\vec{p}_p^f$ ). In the scattering, the spin component perpendicular to the motional direction induces scattering asymmetry. Thus,  $\Lambda p$  spin-spin correlation can be observed as a function of azimuthal angle ( $\phi_{\Lambda p}$ ). The  $\phi_{\Lambda p}$ -distribution can be expressed as

$$N(\phi_{\Lambda p}) = N_0 (1 + r \cdot \alpha_{\Lambda p} \cos \phi_{\Lambda p}), \quad (2)$$

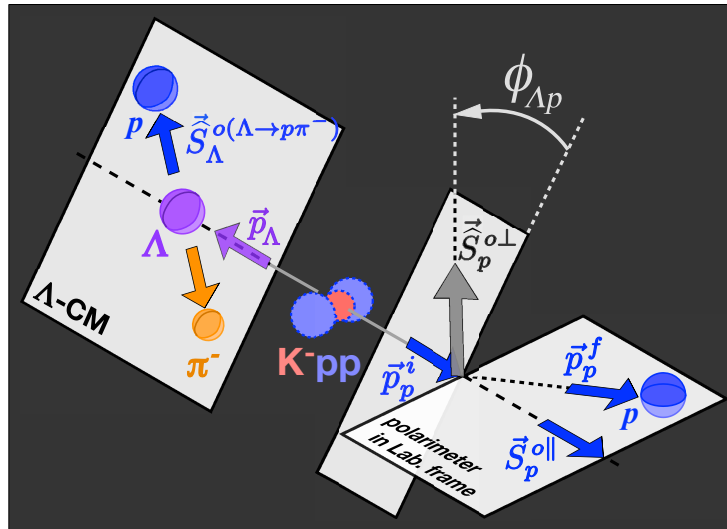


Figure 3: The experimental principle to measure the spin-spin correlation of  $\Lambda p$ . Spin direction of  $\Lambda$  ( $\vec{S}_\Lambda^{o(\Lambda \rightarrow p\pi^-)}$ ) will be measured by weak-decay asymmetry of  $\Lambda$ . Spin direction of proton ( $\vec{S}_p^{o\perp}$ ) will be measured by proton scattering asymmetry in a plastic scintillator.

where  $N_0$  is mean number of events a bin of  $N(\phi_{\Lambda p})$  spectrum, and  $r$  is an asymmetry reduction factor from  $\alpha_{\Lambda p}$  (the factor  $r$  is described in Sec. 5 and Appendix A, in detail).

### 3 Experimental setup

#### 3.1 The K1.8BR beam-line

A schematic drawing of the K1.8BR beam-line is shown in Fig. 4. Note that the figure shows a shortened beam-line configuration, which we have proposed in the E80 [29]. With this configuration,  $K^-$ -beam intensity increases about 1.5 times larger than that with the current K1.8BR configuration. The  $K^-$ -beam is provided by the K1.8BR beam-line, and hardware-level kaon identification is realized by an aerogel Cherenkov counter (AC) located downstream of the last beam-line magnet Q8. More precise kaon identification will be performed using a time-of-flight information obtained from two trigger counters, a beam-line hodoscope tracker (BHT) and time-zero counter (T0). The BHT is a fine segmented hodoscope counter located at the entrance of the D4 magnet. This counter is also used for the kaon beam momentum analysis. The T0 is a segmented hodoscope counter located the exit of the D4 magnet. A beam defining

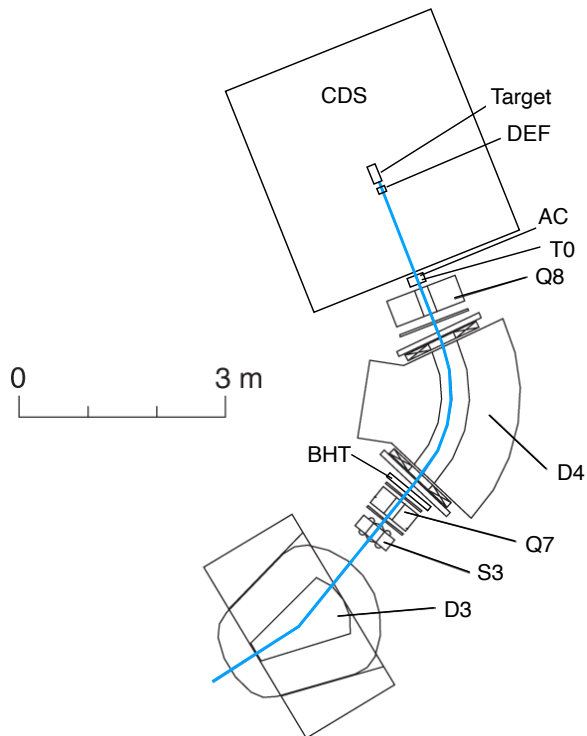


Figure 4: Schematic drawing of the K1.8BR beam-line with a shortened configuration of the beam-line proposed in E80[29].

counter (DEF) is placed in front of the target to select effective kaon beam.

Expected  $K^-$ -beam intensity is  $\sim 320$  k/spill at 90 kW beam-power, considering for the beam expanse and the target size at the focal point. Expected  $K/\pi$  ratio is 1/2, unchanged from present K1.8BR value that ensures trigger rate is in a reasonable range. A similar momentum resolution to the current K1.8BR spectrometer system,  $\Delta p/p \sim 0.2\%$ , is expected.

### 3.2 The cylindrical detector with polarimeter (CDS)

To detect  $\bar{K}NN \rightarrow \Lambda N$  decay as well as spin directions of  $\Lambda$  and proton from “ $K^-pp$ ”  $\rightarrow \Lambda p$  decay, we will use the newly constructed large acceptance cylindrical detector system (CDS), equipped with polarimeter in a superconducting solenoid magnet. The basic components of the CDS have been already summarized in the proposal of E80 experiment [29]. Thus, we only describe the essence of the CDS as follows.

A schematic drawing of the CDS is shown in Fig. 5. A beam drift chamber (BDC) and the DEF are installed as shown in the figure. A cylindrical drift chamber (CDC) is used for tracking of the charged particles from the reaction to measure those momenta. To obtain a larger acceptance coverage, hodoscope counters are located in both barrel and cap parts of the CDS. Each hodoscope counter has thicker plastic scintillator to

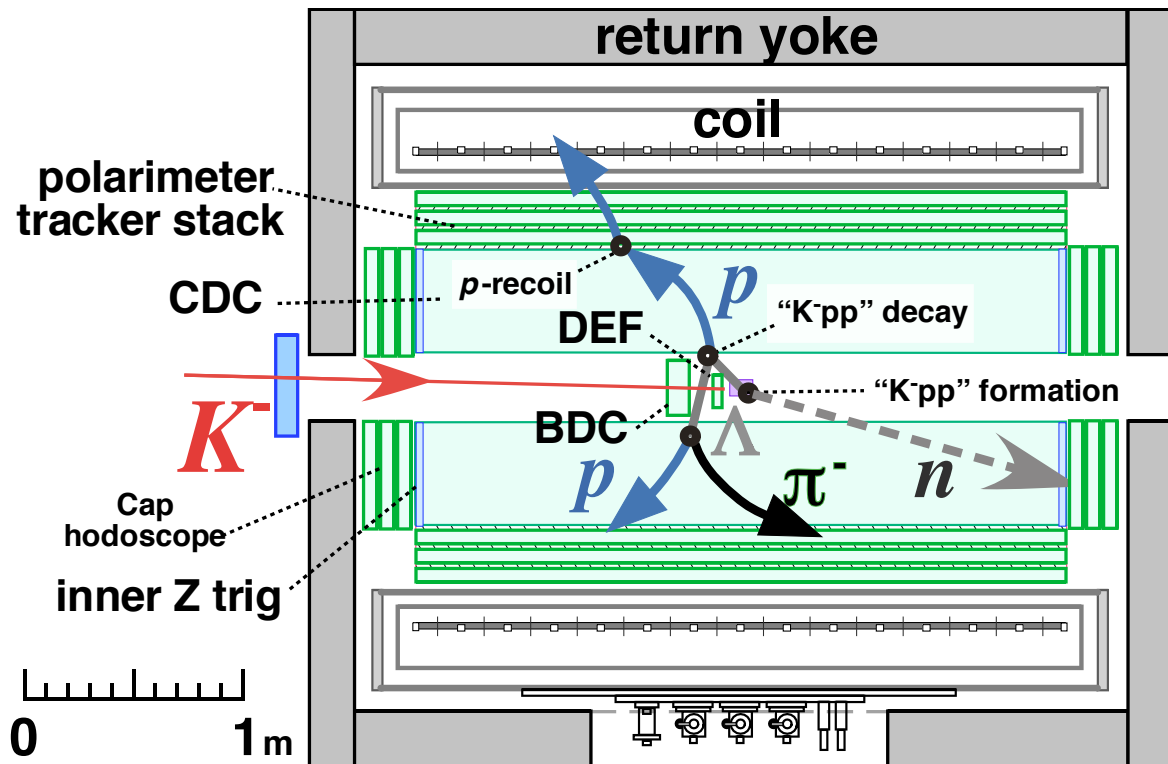


Figure 5: Schematic drawing of the CDS with a typical event.

detect both charged particles and neutrons. The hodoscope in the barrel part (CDH) is used also as a scattering target (polarimeter) to measure proton spin direction. A scattering angle of the proton after passing through the hodoscope will be measured by trackers, which are installed in between each layers of the hodoscope in the barrel part. The trackers will be made of scintillating fibers to obtain a position resolution of 1 mm. All detectors are installed inside the solenoid magnet which provides solenoidal magnetic field of 0.7 T. At the center of the CDS, the experimental target of liquid  ${}^3\text{He}$  is located of which length will be twice longer than that of E15 experiment.

### 3.3 Trigger

A kaon beam trigger (K-beam) will be generated by a coincidence of beam-line hodoscope detectors and veto of the AC; ( $\text{BHT} \otimes \text{T0} \otimes \text{DEF} \otimes \overline{\text{AC}}$ ). In the CDS, three particles should be detected to select  $\Lambda pn$  final state as well as other non-mesonic channel. For mesonic channels, four hits should be detected. Thus, a coincidence of three hits (or more) in hodoscope detectors (CDS-3) can take all the channels in interest. We will take data with a trigger generated by the coincidence; ( $\text{K-beam} \otimes \text{CDS-3}$ ).

A typical trigger rate of the proposed experiment can be estimated from that in the E15 experiment. A trigger rate in E15 was  $\sim 1000/\text{spill}$ , and we doubled both CDS acceptance and  $K^-$ -beam intensity. Thus, a typical trigger rate of the proposed

experiment is expected to be  $\sim 4000$ , that we can handle efficiently enough with an existing DAQ system with more than 90 % efficiency.

## 4 Yield estimation of “ $\bar{K}^0nn$ ” production

As described in Sec. 1, in-flight  $K^- + {}^3\text{He} \rightarrow \Lambda pn$  reaction can be described by  $K^-N \rightarrow \bar{K}N_j$ ,  $\bar{K}NN \rightarrow \Lambda N_k$  successive reaction, in which  $\bar{K}$  is  $\sim$  on-shell. Based on this interpretation, the production cross section of the  $\bar{K}NN$  bound state formation can be estimated from the elementary cross section of the  $K^-N \rightarrow \bar{K}N_j$  reaction as,

$$\sigma_{\bar{K}NN} = R_{\bar{K}NN} \times \sigma_{\bar{K}N} \times C_{NN}^2 \times C_{\bar{K}NN}^2 \times \mathcal{A}_N, \quad (3)$$

where  $R_{\bar{K}NN}$  is the  $\bar{K}NN$  formation probability,  $\sigma_{\bar{K}N}$  is the elementary cross section at  $\theta_N = 0$ ,  $C_{NN}$  and  $C_{\bar{K}NN}$  are Clebsch-Gordan coefficients for isospin coupling of  $NN$  and  $\bar{K}NN$  systems, respectively, and  $\mathcal{A}_N$  is effective proton or neutron number of  ${}^3\text{He}$ .

We summarized each coefficient and production cross section of  $\bar{K}NN$  states in Tab. 2. The elementary cross sections  $\sigma_{\bar{K}N}$  were taken from Ref. [30]. The Clebsch-Gordan coefficients  $C_{NN}$  and  $C_{\bar{K}NN}$  were taken for each  $J^P$  case. The effective proton number  $\mathcal{A}_p$  should be in between  $2^{2/3}$  (in large  $A$  limit) and 2 (in loosely bound limit). The effective neutron number  $\mathcal{A}_n$  is simply assumed to be one. The formation probability  $R_{\bar{K}NN}$  and branching ratios of “ $\bar{K}^0nn$ ”  $\rightarrow \Lambda n$  and “ $K^-pp$ ”  $\rightarrow \Lambda p$  are assumed to be common for the estimation both on “ $\bar{K}^0nn$ ” and “ $K^-pp$ ”, respectively. As listed in the table, the ratio between production cross sections of “ $\bar{K}^0nn$ ” and “ $K^-pp$ ” ( $\sigma_{\bar{K}^0nn}/\sigma_{K^-pp}$ ) is dominantly defined by the spin-isospin selection rule as shown in Eq. 3, and strongly depends on  $J^P$ . If  $\bar{K}NN$  is  $J^P = 0^-$ , the ratio will be as small as 0.13-0.15, namely, “ $\bar{K}^0nn$ ” signal will be much smaller than that of “ $K^-pp$ ”. On the other hand, if  $\bar{K}NN$  is  $1^-$ , yields of “ $\bar{K}^0nn$ ” and “ $K^-pp$ ” are almost in the same level. Therefore, the ratio of production cross sections is a good indicator to deduce  $J^P$ , because the ratio is predominantly defined by the observed elementary cross sections and the spin-isospin selection rule, although it is slightly indirect. Among the parameters, the effective proton number  $\mathcal{A}_p$  could be bit ambiguous, but the  $\mathcal{A}_p$ -dependence is small, and difference of ratios becomes even bigger if we adopt smaller  $\mathcal{A}_p$ .

Table 2: Estimation of production cross section of  $\bar{K}NN$ . For  $C_{NN}^2$ ,  $C_{\bar{K}NN}^2$ ,  $\sigma_{\bar{K}NN}/R_{\bar{K}NN}$ ,  $\sigma_{\bar{K}NN} \cdot BR_{\Lambda N}$ , and  $\sigma_{\bar{K}^0nn}/\sigma_{K^-pp}$ , are described as value( $J^P = 0^-$ ) : value( $J^P = 1^-$ ).  $\sigma_{K^-pp} \cdot BR_{\Lambda p}$  is measured value by E15.

Produced $\bar{K}NN$	“ $\bar{K}^0nn$ ”	“ $K^-pp$ ”	
First step reaction	$K^-p \rightarrow K^-p$	$K^-p \rightarrow \bar{K}^0n$	$K^-n \rightarrow K^-n$
$\sigma_{\bar{K}N}$ (mb/sr)	$\sigma_{K^-p} = 1.8$	$\sigma_{\bar{K}^0n} = 2.4$	$\sigma_{K^-n} = 4.7$
$C_{NN}^2$	1/2 : 1/2	1/2 : 1/2	1 : 0
$C_{\bar{K}NN}^2$	1/3 : 1	1/3 : 1	2/3 : 1
$\mathcal{A}_p = 2^{2/3}, \mathcal{A}_n = 1$			
$\sigma_{\bar{K}NN}/R_{\bar{K}NN}$	0.477 : 1.43	3.77 : 1.91	
$\sigma_{\bar{K}NN} \cdot BR_{\Lambda N}$ ( $\mu\text{b}$ )	1.2 : 7.0	9.3 measured in Ref. [21]	
$\sigma_{\bar{K}^0nn}/\sigma_{K^-pp}$	0.13 : 0.75		
$\mathcal{A}_p = 2, \mathcal{A}_n = 1$			
$\sigma_{\bar{K}NN}/R_{\bar{K}NN}$	0.6 : 1.8	3.9 : 2.4	
$\sigma_{\bar{K}NN} \cdot BR_{\Lambda N}$ ( $\mu\text{b}$ )	1.4 : 7.0	9.3 measured in Ref. [21]	
$\sigma_{\bar{K}^0nn}/\sigma_{K^-pp}$	0.15 : 0.75		

## 5 Sensitivity of expected $\Lambda p$ asymmetry on $\phi_{\Lambda p}$

As it is described in Sec. 2, model independent  $J^P$  determination can be realized by spin-spin correlation factor  $\alpha_{\Lambda p}$  measurement. The most probable  $\Lambda$  spin direction can be estimated by the  $\Lambda \rightarrow p\pi^-$  decay-axis (decay proton motional axis) in  $\Lambda$ 's CM-frame (to avoid the boost effect). For spin measurement of proton from “ $K^-pp$ ”  $\rightarrow \Lambda p$  decay, we plan to use asymmetric nuclear scattering process. The analyzing power  $A_{pC}$  depends on proton kinetic energy  $T_p$  and proton scattering angle  $\theta_p$  as plotted in Fig. 6-(a) [31]. As shown in the figure,  $A_{pC}$  has maximum at  $T_p \sim 250$  MeV at  $\theta_p = 10^\circ$ . On the other hand, the kinetic energy of proton to be measured is simulated as shown in Fig. 6-(b). The energy is slightly lower than the optimal region, but in good range. Taking into account the energy loss effect in polarimeter (CDH) layers, the average analyzing power is estimated to be  $\langle A_{pC} \rangle \sim 0.3$ .

For the proton spin measurement, there are several other points needed to be considered. The nuclear scattering asymmetry is sensitive only to the spin components orthogonal to the motional direction. In fact, spin axis couples strongly to decay axis of “ $K^-pp$ ” due to the angular momentum conservation rule. This means that the amplitude of the nuclear scattering asymmetry depends on the spin orientation referring to the proton motion, that is generated by the momentum transfer  $q$  to “ $K^-pp$ ” at the formation reaction, and the decay of “ $K^-pp$ ”. We should also pay attention to the cyclotron motion and Larmor precession of the spin in the magnetic field of CDS.

Let us first describe the coupling of spin and “ $K^-pp$ ” decay axis. In the case of  $J^P = 0^-$ , angular momentum  $L_{\Lambda p}$  must be canceled by the spin  $S_{\Lambda p}$  to be  $J = 0$ . Therefore, the decay axis of “ $K^-pp$ ”  $\rightarrow \Lambda p$  and  $S_{\Lambda p}$  should be  $\sim$  orthogonal. In the case of  $J^P = 1^-$ , the situation is bit more complicated. The 1/3 of  $\bar{K}NN$  decay to  $S_{\Lambda p} = 0$  ( $\alpha_{\Lambda p} = -1$ ), thus this component is spherical. The other 2/3 component decay to  $S_{\Lambda p} = 1$  ( $\alpha_{\Lambda p} = +1$ ), so the angular momentum  $L_{\Lambda p} = 1$  must be orthogonal to the spin  $S_{\Lambda p} = 1$  to be  $J = 1$ , thus the spin is  $\sim$  parallel to the “ $K^-pp$ ” decay axis (see Appendix B in detail).

Figure 7 shows simulated proton spin distribution at the polarimeter (CDH), where  $\theta_{\vec{s}_p - \vec{v}_p}$  is the opening angle between proton spin direction and its motional axis in the laboratory frame. In the simulation, proton is generated by the decay of “ $K^-pp$ ” having momentum  $q$ , and traced the motion in the spectrometer-magnetic-field, in event-by-event basis. The proton spin is generated according to  $J^P$ , and the spin precession in the field is also considered. As shown in the figure, it is easy to discriminate  $J^P$ , if we can observe  $\theta_{\vec{s}_p - \vec{v}_p}$ . Unfortunately, it is not accessible experimentally.

Alternatively, what we can observe is the spin-spin correlation function between  $\Lambda$  and  $p$  in  $\phi_{\Lambda p}$  direction, in which  $\Lambda \rightarrow p\pi^-$  asymmetry and  $p$ -C scattering asymmetry are convoluted over the entire spin directions experimentally. In the convolution over the spin distribution, a weighting factor  $\sin^2 \theta_{\vec{s}_p - \vec{v}_p}$  appears as for the effective asymmetry amplitude between  $\Lambda$  and  $p$  spin orientation (see Appendix A). This factor is inset as

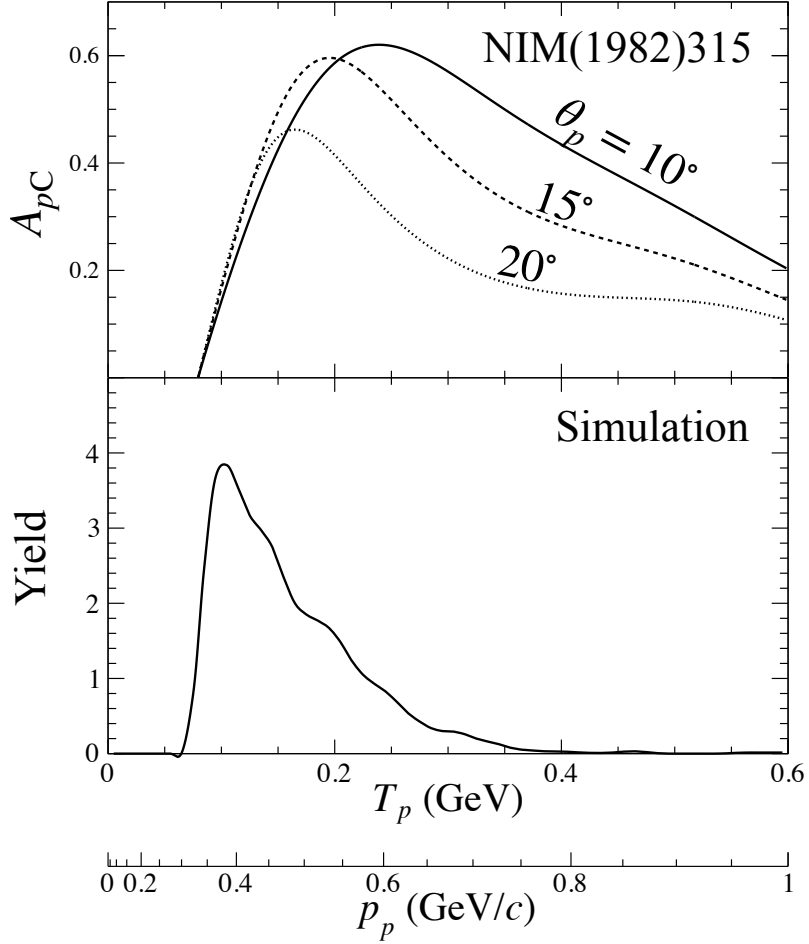


Figure 6: (a) Analyzing power of proton-carbon scattering ( $A_{pC}$ ) [31]. (b) Kinetic energy (momentum) distribution of proton from  $\bar{K}NN$  decay at the most inner polarimeter in the barrel part.

green line in Fig. 7. As shown in the figure, spin distribution of  $J^P = 0^-$  and  $\sin^2 \theta_{\vec{s}_p - \vec{v}_p}$  matches rather nicely, so the  $\Lambda$ - $p$  spin-spin correlation measurement is relatively easy. On the other hand, in the case of  $J^P = 1^-$ , overlap with  $\sin^2 \theta_{\vec{s}_p - \vec{v}_p}$  is smaller than that of  $J^P = 0^-$ , but it helps to discriminate the  $J^P$  by the  $\phi_{\Lambda p}$  asymmetry measurement.

Figure 8 shows the  $\phi_{\Lambda p}$  asymmetry based on the event-by-event simulation to take into account all the effects appeared on the spin measurement including  $\Lambda$  precession in the field. As described,  $\phi_{\Lambda p}$ -distribution asymmetry is smaller than  $\alpha_{\Lambda p}$ , and the correlation reduction factor is summarized as  $r$ -factor. Expected asymmetries  $r\alpha_{\Lambda p}$  were estimated to be  $\sim 0.65$  and  $\sim 0.01$  for  $J^P = 0^-$  and  $1^-$  cases, respectively. Note that in-situ evaluation and calibration on  $r$  factor is doable utilizing the proton spin measurement of  $\Lambda \rightarrow p\pi^-$  decay, by the correlation between the decay axis and asymmetric scattering of that proton. Therefore, we can deduce the absolute  $\alpha_{\Lambda p}$  value

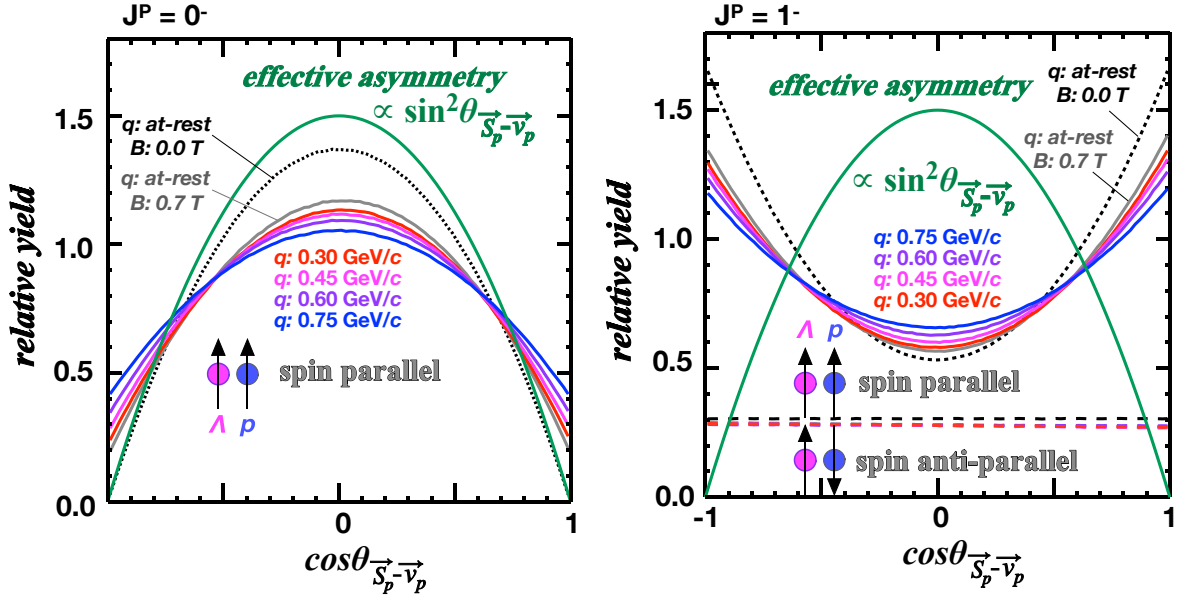


Figure 7:  $\cos\theta_{\vec{s}_p - \vec{v}_p}$  distribution for (left)  $J^P = 0^-$  and (right)  $J^P = 1^-$ . The black dotted lines show distribution without magnetic field nor boost of  $K^-pp$ . The colored lines show distribution including both magnetic field and boost of  $K^-pp$ . The green line shows effective asymmetry factor for proton spin measurement by nuclear scattering.

with much smaller systematical error than the statistical one.

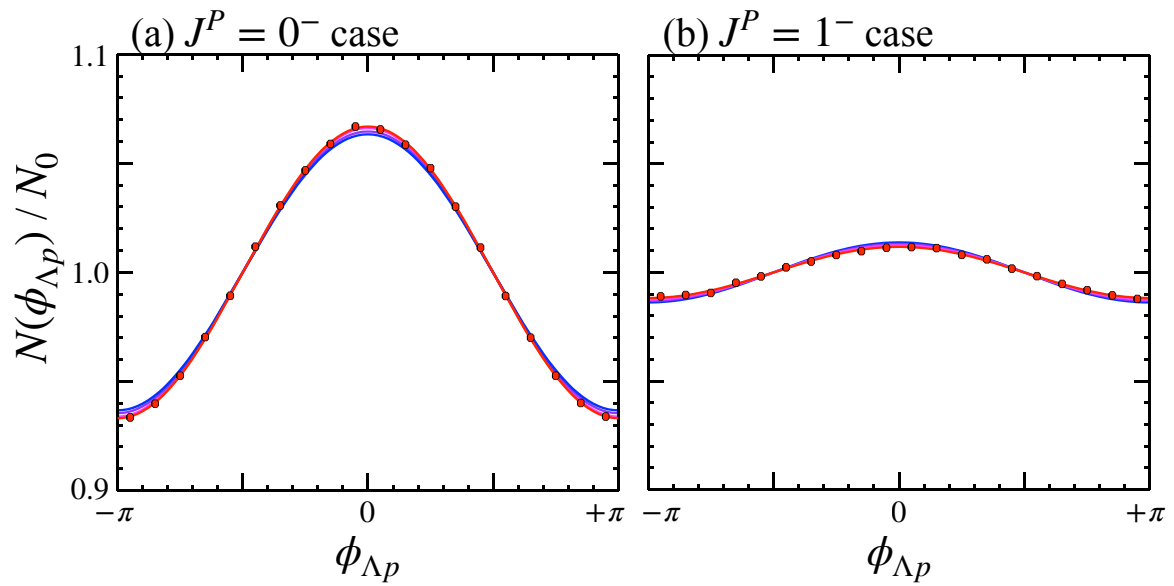


Figure 8:  $\phi_{\Lambda p}$  distribution for (left)  $J^P = 0^-$  and (right)  $J^P = 1^-$ . The vertical axes are scaled by  $N_{bin} / \int N(\phi_{\Lambda p})$ , so as to make the distribution  $1 + r\alpha_{\Lambda p} \cos \phi_{\Lambda p}$ .

## 6 Expected spectra

### 6.1 Detection of isospin doublet, “ $\bar{K}^0 nn$ ”, and isospin symmetry study by the mass determination

The yield of the “ $\bar{K}^0 nn$ ” to decay into  $\Lambda n$  can be estimated from the production cross section of “ $\bar{K}^0 nn$ ” ( $\sigma_{\bar{K}^0 nn} \cdot \text{BR}_{\Lambda n}$ ) at luminosity  $\mathcal{L}$  as,

$$N_{\bar{K}^0 nn} = \sigma_{\bar{K}^0 nn} \cdot \text{BR}_{\Lambda n} \times \mathcal{L}, \quad (4)$$

$\sigma_{\bar{K}^0 nn} \cdot \text{BR}_{\Lambda n}$  was estimated to be from 1.2 to 1.4  $\mu\text{b}$  for  $J^P = 0^-$  case with the range of effective proton number ( $2^{2/3} \leq \mathcal{A}_p \leq 2$ ).  $\mathcal{L}$  per week can be estimated as,

$$\mathcal{L}_{\text{week}} = N_{K^-} \times N_{^3\text{He}} \times \varepsilon_{\text{Beam}} \times \varepsilon_{\text{DAQ}} \times \varepsilon_{\text{Facility}} \times (60 \times 60 \times 24 \times 7/5.2), \quad (5)$$

where  $N_{K^-} = 320$  k/spill (5.2 s repetition cycle with shortened configuration of K1.8BR beam-line) is the number of  $K^-$ -beam in a spill,  $N_{^3\text{He}} = 3.4 \times 10^{23}$  /cm<sup>2</sup> is the number of <sup>3</sup>He-target nucleus,  $\varepsilon_{\text{Beam}} = 0.55$  is an analysis efficiency for the beam (realized in the E15 experiment),  $\varepsilon_{\text{DAQ}} = 0.9$  is a DAQ efficiency, and  $\varepsilon_{\text{Facility}} = 0.9$  is an uptime ratio of the J-PARC accelerator. With these values,  $\mathcal{L}_{\text{week}}$  is expected to be 5.6 nb<sup>-1</sup>/week (corresponding to 37 GK<sup>-</sup> on target and 81 kW · week). As a result, expected numbers of formation reactions of “ $\bar{K}^0 nn$ ”  $\rightarrow \Lambda n$  and “ $K^- pp$ ”  $\rightarrow \Lambda p$  are as summarized in Tab. 3. In this estimation, we assumed that we can double the amount of <sup>3</sup>He target compared to that of E15. The expected number of “ $\bar{K}^0 nn$ ” of  $J^P = 0^-$  slightly ranges due to ambiguity of the effective proton number  $\mathcal{A}_p$  as described in Sec.4.

Table 3: Expected number of formation reaction per week (corresponding to  $\mathcal{L} = 5.6$  nb<sup>-1</sup> and 81 kW · week) without taking into account acceptance, nor analysis efficiency. The estimated production cross section of “ $\bar{K}^0 nn$ ” with  $J^P = 0^-$  slightly ranges due to ambiguity of effective proton number  $\mathcal{A}_p$  ( $=2^{2/3} \sim 2$ ). See Tab. 2 for the detail of the estimation.

Produced $\bar{K}NN$	$J^P$	$\sigma_{\bar{K}NN} \cdot \text{BR}_{\Lambda N}$	$N_{\bar{K}NN \rightarrow \Lambda N}$
“ $\bar{K}^0 nn$ ”	$0^-$	1.2 ~ 1.4 $\mu\text{b}$	6480 ~ 7840
	$1^-$	7.0 $\mu\text{b}$	31360
” $K^- pp$ ”	-	9.3 $\mu\text{b}$ [21]	52080

To obtain an expected spectrum of the “ $\bar{K}^0 nn$ ”, we performed a Monte Carlo simulation. As described in Sec. 1, in-flight  $K^- + ^3\text{He} \rightarrow \Lambda pn$  reaction can be described by  $K^- N \rightarrow \bar{K} N_j$ ,  $\bar{K} NN \rightarrow \Lambda N_k$  successive reaction, in which  $\bar{K}$  is  $\sim$  on-shell. Therefore, we generated following four processes to estimate events-distribution of the  $\Lambda pn$  final state.

- “ $\bar{K}^0nn$ ” production (decay into  $\Lambda n$ ),  $\sigma_{\bar{K}^0nn} \cdot \text{BR}_{\Lambda n} = 1.2 \sim 1.4 \mu\text{b}$  ( $J^P = 0^-$  assumption)
- quasi-free reaction going to  $\Lambda n$  channel ( $\text{QF}_{\Lambda n}$ ),  $\sigma_{\text{QF}_{\Lambda n}} = 3.6 \sim 4.1 \mu\text{b}$
- “ $K^-pp$ ” production (decay into  $\Lambda p$ ),  $\sigma_{K^-pp} \cdot \text{BR}_{\Lambda p} = 9.3 \mu\text{b}$
- quasi-free reaction going to  $\Lambda p$  channel ( $\text{QF}_{\Lambda p}$ ),  $\sigma_{\text{QF}_{\Lambda p}} = 10.7 \mu\text{b}$

In the former two processes, proton is knocked out, and  $\Lambda n$  are produced as decay products of the “ $\bar{K}^0nn$ ” bound state or as a result of the  $K^-$ -absorption to the residual  $NN$ . The cross section of the  $\text{QF}_{\Lambda n}$  was estimated to be  $3.6 \sim 4.1 \mu\text{b}$  by the same manner described in Sec. 4, where the range of the cross section comes from ambiguity of the effective proton number  $\mathcal{A}_p$ . The latter two processes are observed in the E15 [21].

Thanks to the enlarged acceptance, “ $\bar{K}^0nn$ ” formation detection can be realized using  $\Lambda p$  detected events, since the missing neutron can be kinematically identified for the  $\Lambda pn$  final state. In a count base,  $\Lambda n$ -pair spectrum using  $\Lambda p$  detection mode gives bigger yield than that of direct  $\Lambda n$  detection mode, even at the present improved neutron detection capability (see Appendix C). Thus, we plotted  $\Lambda n$ -pair spectra using  $\Lambda p$  detected events as shown in Fig. 9, by assuming  $J^P$  of  $\bar{K}NN$  doublet to be  $0^-$  (natural, but much severe assumption for “ $\bar{K}^0nn$ ” detection). Even with the  $\Lambda p$  mode, we need as long as 8 weeks beam-time. In the 2D distribution shown in Fig. 9-(a),

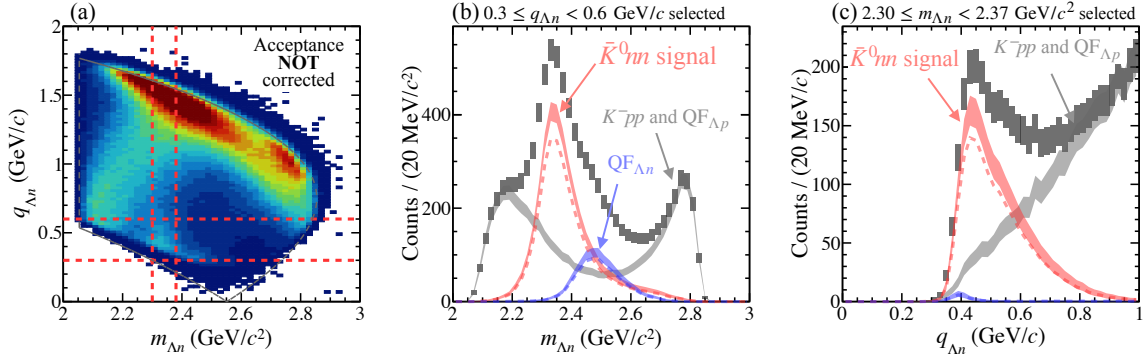


Figure 9: Expected result for the “ $\bar{K}^0nn$ ” measurement, assuming  $J^P$  of “ $K^-pp$ ” observed in E15 to be  $0^-$ . (a) two-dimensional distribution on the invariant-mass of  $\Lambda n$  ( $m_{\Lambda n}$ ) and momentum transfer to  $\Lambda n$  ( $q_{\Lambda n}$ ). (b) Projection spectrum on the  $m_{\Lambda n}$  axis by selecting  $0.3 \leq q_{\Lambda n} < 0.6$  GeV/c region. (c) Projection spectrum on the  $q_{\Lambda n}$  axis by selecting  $2.3 \leq m_{\Lambda n} < 2.37$  GeV/c<sup>2</sup> region. The dotted histograms in the projections show the case of the expected yield to be minimum with smaller effective proton number  $\mathcal{A} = 2^{2/3}$ .

a strong events-concentration from background processes is seen in larger  $q_{\Lambda n}$  region above 1 GeV/c, but it is well separated from the region of interest. On the other

hand, in the lower  $q_{\Lambda n}$  region, relatively weak but clear signal of the “ $\bar{K}^0 nn$ ” formation is expected. As shown in Fig. 9-(b), the “ $\bar{K}^0 nn$ ” formation signal can be seen more clearly when we select lower momentum transfer region.

Figure 10 shows comparison between expected results with  $J^P = 0^-$  and  $1^-$  assumptions. As shown in Fig. 10, detection of “ $\bar{K}^0 nn$ ” formation signal is much more

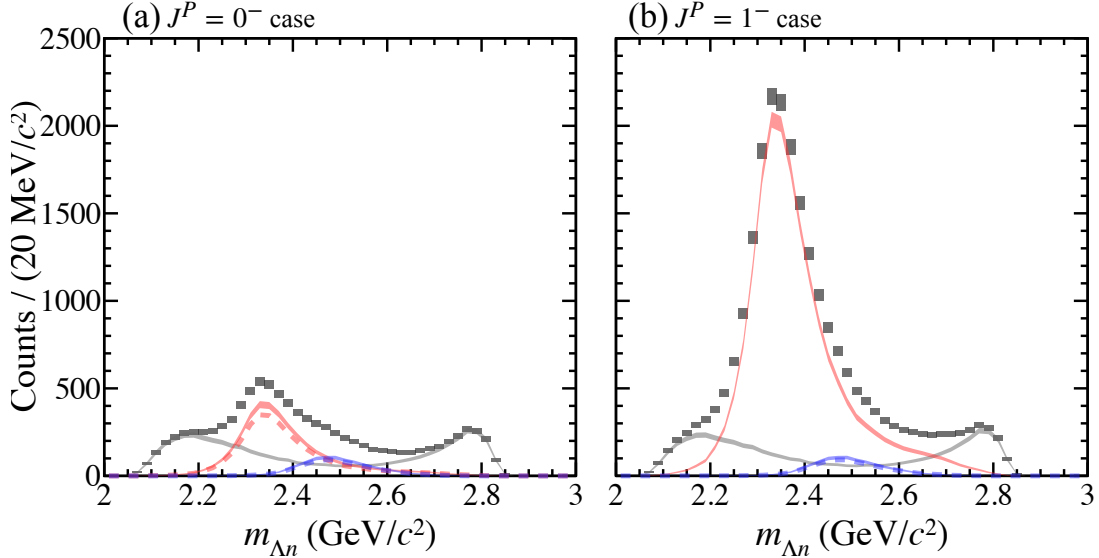


Figure 10: Expected invariant-mass spectra of  $\Lambda n$ -pair by selecting  $0.3 \leq q_{\Lambda n} < 0.6$  GeV/c region for (a)  $J^P = 0^-$  (same as Fig. 9-(b)) and (b)  $J^P = 1^-$ . In the case of  $J^P = 0^-$ , expected yield slightly changed if  $\mathcal{A} = 2^{2/3}$  as shown by dotted histograms.

easy, if  $J^P$  of  $\bar{K}NN$  isospin doublet is  $1^-$ .

The present  $\Lambda p$  event mode analysis has statistical advantage in “ $\bar{K}^0 nn$ ” detection, compared to  $\Lambda p$  mode. However, it should be noted that it does not mean the less importance of  $\Lambda n$  mode analysis. In fact, the momentum transfer spectrum given in Fig. 9 has a sharp cutoff at  $\sim 0.4$  GeV/c. This cutoff doesn’t come from physics, but from the CDS acceptance (see Appendix C). We wish to stress that the observation of entire kinematical region is inevitable to reach clear understanding of the reaction mechanism and dynamics of the  $\bar{K}NN$  bound state formation.

## 6.2 Measurement of $\alpha_{\Lambda p}$

Figure 11 shows expected spectra of “ $K^- pp$ ” measurement with 8 weeks beam-time. We select the “ $K^- pp$ ” signal rather loosely as shown by red box in Fig. 11-(a) to keep an enough statistics for  $\alpha_{\Lambda p}$  measurement. With this signal window, we cannot exclude the backgrounds severely, but no spin correlation between  $\Lambda$  and proton is expected. Thus, background subtraction can be simple.

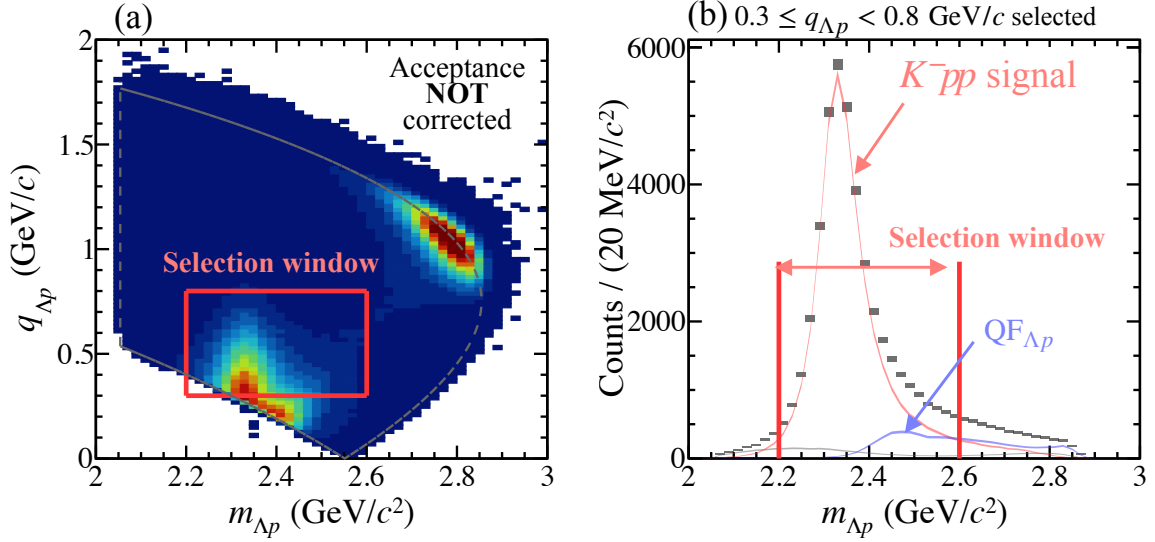


Figure 11: Expected spectra of “ $K^-pp$ ” measurement with 8 weeks beam-time. (a) two-dimensional distribution on the invariant-mass of  $\Lambda p$  ( $m_{\Lambda p}$ ) and momentum transfer to  $\Lambda p$  ( $q_{\Lambda p}$ ). (b) Projection spectrum on the  $m_{\Lambda p}$  axis by selecting  $0.3 \leq q_{\Lambda p} < 0.8$  GeV/ $c$  region. The red box in (a) and red lines in (b) are selection window for  $\alpha_{\Lambda p}$  measurement.

Figure 12 shows proton scattering angle  $\theta_p$  distribution at the polarimeter. A peak at  $\theta_p \sim 0^\circ$  corresponds to multiple-scattering events which does not have any asymmetry. A tail component in larger  $\theta_p$ -region is dominant in  $p$ -C scattering events having good proton spin sensitivity. The multiple-scattering peak becomes wider if detector resolutions are included, we can select reasonable number of the spin-sensitive asymmetric  $p$ -C scattering with 1 mm spatial resolution as shown in the figure.

Figure 13 shows estimated  $\phi_{\Lambda p}$  distributions for each  $J^P$ . The red lines in the figure show fit result of the simulated distribution with  $1 + A \cos \phi_{\Lambda p}$ , and the red bands correspond to fitting error ( $1\sigma$ ). We would exclude  $J^P = 1^-$  hypothesis more than 95% confidence level only by the  $\alpha_{\Lambda p}$  measurement. By combining with the  $\sigma_{\bar{K}^0 nn} / \sigma_{K^- pp}$ , we would provide an conclusive result to determine  $J^P$ .

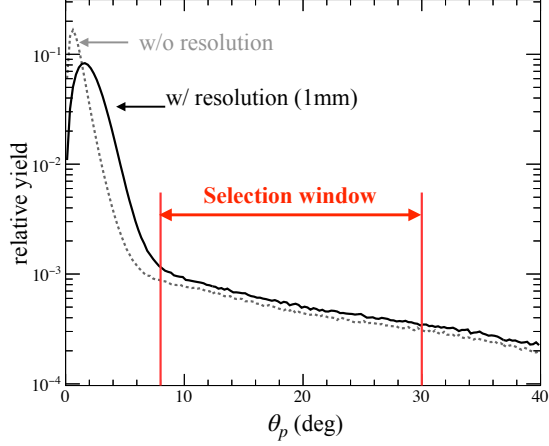


Figure 12: Expected  $\theta_p$ -distribution with (black) and without (gray dotted) detector resolution (1mm for tracker in the polarimeter). Spin sensitivity in the multiple scattering dominant region (very forward region) is quite weak, so we set the selection window as indicated by the led lines.

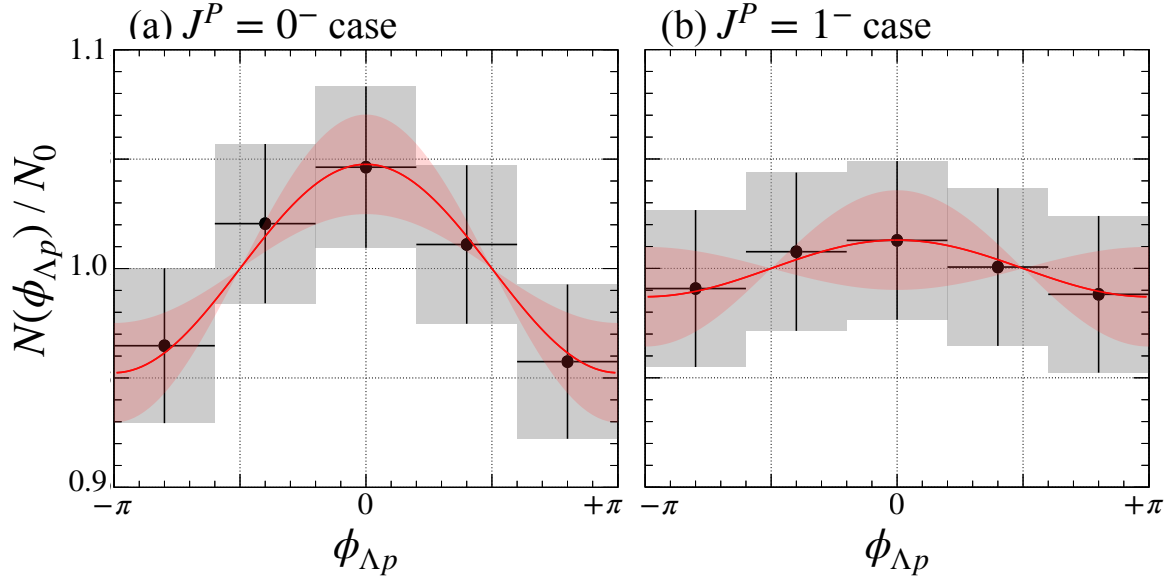


Figure 13: Expected  $\phi_{\Lambda p}$ -distribution for “ $K^- pp$ ”  $\rightarrow \Lambda p$  decay with 8 weeks beam-time for (a)  $J^P = 0^-$  and (b)  $J^P = 1^-$ . The red line and red band shows fitting result and  $1\sigma$  region.

## 7 Beam time request

As we described in the previous section, 8 weeks beam-time with 90 kW beam power (648 kW · week) is necessary to confirm  $\bar{K}NN$  as an isospin doublet of  $I = 1/2$ , and to determine  $J^P$ .

The main part of the detector system are commonly used with E80 experiment, so that it will be ready at the same time as E80 experiment in 2025. Additionally, we will construct polarimeter system and purchase additional 300L gaseous  $^3\text{He}$  for the proposed experiment. Although, we can finish the preparation until E80 experiment will be started.

## 8 Summary of objectives

We propose a new experiment to investigate the fundamental property of the simplest kaonic nuclear bound state,  $\bar{K}NN$  at J-PARC K1.8BR beam-line. In the experiment, we will observe the  $I_z = -1/2$   $\bar{K}NN$  state, “ $\bar{K}^0nn$ ”, and determine the most fundamental quantum number, spin-parity of the  $\bar{K}NN$  state, utilizing much improved statistics in “ $K^-pp$ ”. “ $\bar{K}^0nn$ ” production will be observed by analyzing  $\Lambda n$  invariant-mass and momentum transfer to  $\Lambda n$ . To deduce  $J^P$  in a conclusive manner, we will measure both production cross sections ratio between “ $\bar{K}^0nn$ ” and “ $K^-pp$ ”, and spin-spin correlation of  $\Lambda p$ -pair from the “ $K^-pp$ ” decay at the same time. As a result of  $\sim 4\pi$  coverage of the CDS, doubled  $^3\text{He}$ -target, and improved kaon beam intensity by primary beam power and shortened beam-line geometry, we can obtain sufficient statistics for these measurements with 8 weeks beam-time. We can also provide informations on branching ratio and total production cross section of the  $\bar{K}NN$ , from which we can efficiently study the internal sub-structure caused by  $\Lambda(1405)$  resonance in the system.

In the experiment we can detect both  $\Lambda p$  and  $\Lambda n$  pairs in the  $K^- + ^3\text{He} \rightarrow \Lambda pn$  reaction, which enables us to investigate the reaction kinematics in whole kinematically allowed region. From the measurement of  $\Lambda pn$  as well as  $\Sigma^- pp$  final states, we can confirm our interpretation that the  $K^- + ^3\text{He} \rightarrow YN_1N_2$  reaction (final state with minimal baryon) can be entirely described by  $K^-N \rightarrow \bar{K}N_j$  followed by  $\bar{K}NN \rightarrow \Lambda N_k$  successive reaction, which lead us to full understanding of the reaction dynamics of elementary formation mechanism of kaonic nuclear bound state.

Together with J-PARC E80 and successive measurements, we wish to open a new doorway to access unexplored physical region of the QCD phase diagram at low-temperature and high-density. In that region, we are expecting rich physics, because hadron properties may change substantially as a function of chiral order parameter  $|\langle \bar{q}q \rangle|$ . Thus, hadron mass can be largely modified due to the recovery of spontaneous chiral-symmetry breaking of the vacuum ( $\bar{q}q$ -condensation) due to the high matter density. We may also access equation-of-state (EOS) of hadronic matter, if we can separate the  $I_{\bar{K}N} = 0$  attraction and  $NN$  short-range repulsion in the system. Such a high-density nuclear matter implied by the E15 experimental data has never been

observed before. The systematic study in future, we may have vital information to understand the puzzle of heavy neutron star. In an extreme, hadron may lose its identity as a particle in a high density system. If we can observe the precursor effect of particle dissociation, *i.e.*, transition from hadronic matter to QCD-matter on the spot, impact will be huge. In parallel to the experimental study, we wish to establish the theoretical framework to extend the physics program to be opened in future.

## References

- [1] R. H. Dalitz and S. F. Tuan. *Ann. Phys.*, 8(1):100–118, 1959.
- [2] R. H. Dalitz, T. C. Wong, and G. Rajasekaran. *Phys. Rev.*, 153(5):1617–1623, jan 1967.
- [3] T. Yamazaki and Y. Akaishi. *Phys. Lett. B*, 535(1-4):70–76, 2002.
- [4] Y. Akaishi and T. Yamazaki. *Phys. Rev. C*, 65(4):044005, 2002.
- [5] Y. Ikeda and T. Sato. *Phys. Rev. C*, 76(3):1–10, 2007.
- [6] N. V. Shevchenko, A. Gal, and J. Mareš. *Phys. Rev. Lett.*, 98(8):1–4, 2007.
- [7] N. V. Shevchenko, A. Gal, J. Mareš, and J. Révai. *Phys. Rev. C*, 76(4), 2007.
- [8] A. Doté, T. Hyodo, and W. Weise. *Nucl. Phys. A*, 804(1-4):197–206, 2008.
- [9] S. Wycech and A. M. Green. *Phys. Rev. C*, 79(1):1–15, 2009.
- [10] A. Doté, T. Hyodo, and W. Weise. *Phys. Rev. C*, 79(1):1–16, 2009.
- [11] Y. Ikeda and T. Sato. *Phys. Rev. C*, 79(3), 2009.
- [12] N. Barnea, A. Gal, and E.Z. Liverts. *Phys. Lett. B*, 712(1-2):132–137, may 2012.
- [13] M. Bayar and E. Oset. *Phys. Rev. C*, 88(4):1–8, 2013.
- [14] J. Révai and N. V. Shevchenko. *Phys. Rev. C*, 90(3):1–6, 2014.
- [15] T. Sekihara, E. Oset, and A. Ramos. *Prog. of Theor. and Exp. Phys.*, 2016(12):123D03, dec 2016.
- [16] A. Doté, T. Inoue, and T. Myo. *Phys. Rev. C*, 95(6):1–5, 2017.
- [17] S. Ohnishi et al. *Phys. Rev. C*, 95(6):065202, jun 2017.
- [18] A. Doté, T. Inoue, and T. Myo. *Phys. Lett. B*, 784:405–410, sep 2018.
- [19] Y. Sada et al. *Prog. Theor. Exp. Phys.*, 2016(5):051D01, may 2016.

- [20] S. Ajimura et al. *Phys.Lett. B*, 789:620–625, 2019.
- [21] T. Yamaga et al. *Phys. Rev. C*, 102(4):044002, oct 2020.
- [22] T. Yamazaki et al. *Phys. Rev. Lett.*, 104(13):132502, apr 2010.
- [23] Yudai Ichikawa et al. *Prog. Theor. Exp. Phys.*, 2015(2):21D01–0, feb 2015.
- [24] M. Agnello et al. Evidence for a kaon-bound state K-pp produced in K- absorption reactions at rest. *Phys. Rev. Lett.*, 94(21):212303, jun 2005.
- [25] T. Yamazaki and Y. Akaishi. *Phys. Rev. C*, 76(4):1–16, 2007.
- [26] T. Sekihara, J. Yamagata-Sekihara, D. Jido, and Y. Kanada-En’Yo. *Physical Review C - Nuclear Physics*, 86(6):1–17, 2012.
- [27] N. V. Shevchenko and J. Révai. *Phys. Rev. C*, 90(3):1–8, 2014.
- [28] N. V. Shevchenko. *Few-Body Systems*, 61(3):1–7, 2020.
- [29] S. Fuminori et al. J-PARC P80 proposal.
- [30] T. Kishimoto. *Phys. Rev. Lett.*, 83(23):4701–4704, dec 1999.
- [31] R. D. Ransome et al. *Nuclear Instruments and Methods In Physics Research*, 201(2-3):315–321, oct 1982.

## A $\phi_{\Lambda p}$ -distribution and $r$ representation

Let us calculate asymmetry reduction factor  $r$  mathematically. Figure 14 illustrates a spin orientation in an event measurement. For simplicity, we calculate only for

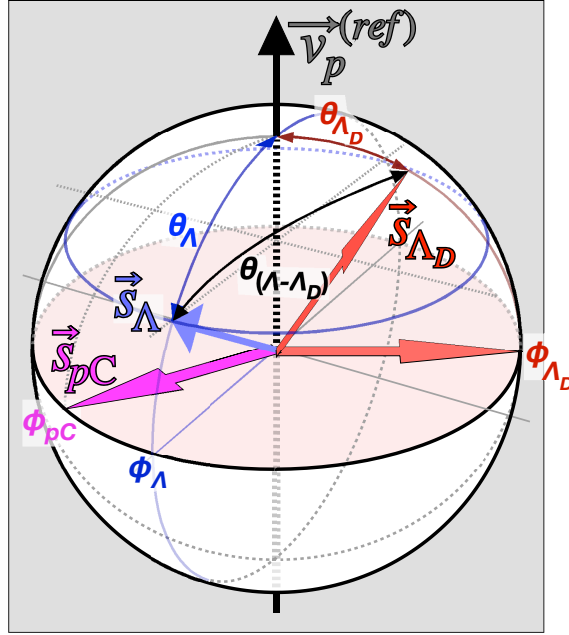


Figure 14: A spin orientation in the measurement. All are normalized vectors,  $\vec{S}_\Lambda$  is true spin direction of  $\Lambda$ ,  $\vec{S}_{\Lambda_D}$  is estimated spin direction of  $\Lambda$  by  $\Lambda \rightarrow p\pi^-$  decay (decayed proton's motional vector in  $\Lambda$ 's CM frame), and  $\vec{S}_{pC}$  is estimated spin direction of proton by  $p$ -C scattering (vector product of protons motional vectors before and after scattering,  $\vec{v}_p^{ref} \times \vec{v}'_p$ , so  $\vec{S}_{pC}$  is orthogonal to  $\vec{v}_p^{ref}$ ). The  $\theta_\Lambda$  given in this figure corresponds to  $\theta_{\vec{S}_p - \vec{v}_p}$  (for  $\alpha_{\Lambda p} = +1$  in the main text).

$\alpha_{\Lambda p} = +1$  case, in which both  $\Lambda p$  spins are parallel (same), but all the calculation is the same for  $\alpha_{\Lambda p} = -1$  component, except for the sign. In the figure, we set the proton's motional vector ( $\vec{v}_p^{ref}$ ) as the reference axis. The measured azimuthal angle difference,  $\phi_{\Lambda p}$  is obtained as  $\phi_{\Lambda p} = \phi_{\Lambda_D} - \phi_{pC}$ .

In the measurement, a probability to have a specific spin orientation is written as,

$$P = f_{\vec{S}_\Lambda}(\theta_\Lambda, \phi_\Lambda) (1 + \alpha_- \cos \theta_{(\Lambda - \Lambda_D)}) (1 + A_{pC} \sin \theta_\Lambda \cos(\phi_\Lambda - \phi_{pC})), \quad (6)$$

where  $f_{\vec{S}_\Lambda}(\theta_\Lambda, \phi_\Lambda)$  describes  $\vec{S}_\Lambda$  distribution normalized as  $\int f d\Omega = 1$ , the first term represents  $\vec{S}_\Lambda \cdot \vec{S}_{\Lambda_D}$  ( $= \cos \theta_{(\Lambda - \Lambda_D)}$ ) probability density of  $\Lambda \rightarrow p\pi^-$  decay, and the second term is azimuthal angle probability density of  $p$ -C scattering with analyzing power of  $A_{pC}$ , formed by proton spin polarization of  $\sin \theta_\Lambda$  as illustrated in the figure.

From haversine formula,

$$P(\theta_\Lambda, \phi_\Lambda, \theta_{\Lambda_D}, \phi_{\Lambda_D}) = \frac{f_{\vec{S}_\Lambda}(\theta_\Lambda, \phi_\Lambda)}{4\pi} (1 + \alpha_- [\cos \theta_\Lambda \cos \theta_{\Lambda_D} + \sin \theta_\Lambda \sin \theta_{\Lambda_D} \cos(\phi_\Lambda - \phi_{\Lambda_D})]) \cdot (1 + A_{pC} \sin \Lambda \cos(\phi_\Lambda - \phi_{pC})). \quad (7)$$

Because  $p$ -C scattering do not have any spin sensitivity in  $\cos \theta_{\Lambda_D}$  direction, thus we simply integrated out as,

$$\begin{aligned} \int P(\theta_\Lambda, \phi_\Lambda, \theta_{\Lambda_D}, \phi_{\Lambda_D}) d(\cos \theta_{\Lambda_D}) &= P(\theta_\Lambda, \phi_\Lambda, \phi_{\Lambda_D}) \\ &= \frac{2f_{\vec{S}_\Lambda}(\theta_\Lambda, \phi_\Lambda)}{4\pi} \left(1 + \frac{\pi}{4} \alpha_- \sin \theta_\Lambda \cos(\phi_\Lambda - \phi_{\Lambda_D})\right) \cdot (1 + A_{pC} \sin \Lambda \cos(\phi_\Lambda - \phi_{pC})) \\ &= \frac{2f_{\vec{S}_\Lambda}(\theta_\Lambda, \phi_\Lambda)}{4\pi} \left[1 + \frac{\pi}{4} \alpha_- \sin \theta_\Lambda \cos(\phi_\Lambda - \phi_{\Lambda_D}) + A_{pC} \sin \Lambda \cos(\phi_\Lambda - \phi_{pC}) \right. \\ &\quad \left. + \frac{\pi}{4} \alpha_- A_{pC} \sin^2 \theta_\Lambda \cos(2\phi_\Lambda - \phi_{\Lambda_D} - \phi_{pC}) + \frac{\pi}{4} \alpha_- A_{pC} \sin^2 \theta_\Lambda \cos(\phi_{\Lambda_D} - \phi_{pC})\right]. \end{aligned} \quad (8)$$

One needs to integrate the equation over  $\theta_\Lambda$  and  $\phi_\Lambda$ , to reach the expression of the asymmetry reduction factor  $r$  in  $N(\phi_{\Lambda p}) = N_0(1 + r \cdot \alpha_{\Lambda p} \cos \phi_{\Lambda p})$ . Without specifying the spin distribution function  $f$ , one can go one-step further by considering the physical meaning of each term. After the integration, the first term is independent to angle and gives average of the probability, the last term depends only on  $\phi_{\Lambda p}$ , and all the other terms depends on angles independent to  $\phi_{\Lambda p}$ , thus must be integrated-out to be zero. Hence,  $r$  can be given as,

$$r = \frac{\pi}{4} \alpha_- A_{pC} \int d\Omega_\Lambda f_{\vec{S}_\Lambda} \sin^2 \theta_\Lambda. \quad (9)$$

The spin distribution function  $f$  depends on  $J^P$  and  $\Lambda p$  spin  $S_{\Lambda p}$ . Moreover, the reference vector  $\vec{v}_p^{ref}$  of the  $f$  changes due to the momentum kick caused by the momentum transfer  $q$  to  $\bar{K}NN$ . During the particle motion before the decay or scattering,  $\vec{v}_p^{ref}$ ,  $\vec{S}_p$  and  $\vec{S}_\Lambda$  change even further, due to the magnetic field of CDS. Therefore, the factor  $r$  can only be estimated by the detailed simulation in a specific experimental condition, unfortunately. However, the validity of the spin simulation can be secured quite nicely by using  $\Lambda \rightarrow p\pi^-$  decay. Because, in the weak decay,  $p$  spin direction is well known, so we can examine and self-calibrate the spin simulation/analysis code using data given by the same experimental setup.

As for the reference,  $r$  factor number for uniform spin distribution case ( $f = 1/4\pi$ ) at  $q = 0$  without magnetic field can be given as,

$$r = \frac{\pi}{12} \alpha_- A_{pC} \approx 0.057, \quad (10)$$

with  $\alpha_- = 0.72$  and  $A_{pC} = 0.3$ .

## B $\Lambda p$ spin distribution referring to the “ $K^-pp$ ” decay-axis

Let us describe spin distribution referring to the “ $K^-pp$ ” decay-axis in specifically. As we described in Sec. 2,  $J^P$  of “ $K^-pp$ ” is conserved in the decay, thus

$$S_{\Lambda p} \otimes L_{\Lambda p} = J, \quad (11)$$

with  $L_{\Lambda p} = 1$  ( $P$ -wave decay), for both  $0^-$  and  $1^-$ .

When  $S_{\Lambda p} = 1$ , it should couple with orbital angular momentum ( $Y_1^m$ , that defines decay axis) of  $\Lambda p$  in a specific manner due to the conservation rule, and this coupling brings strong correlation between spin-direction and decay-axis of the “ $K^-pp$ ”. Figure 15 shows spin orientation in  $\bar{K}NN$   $J^P = 0^-$ . To be  $J_z = 0$ ,  $L_{\Lambda p} = |1, \pm 1\rangle$  should couple with  $S_{\Lambda p} = |1, \mp 1\rangle$ , respectively (Fig.15-(a) and (b)), thus  $S_{\Lambda p}$  and decay-axis are orthogonal. On the other hand, in the case of  $L_{\Lambda p} = |1, 0\rangle$  and  $S_{\Lambda p} = |1, 0\rangle$ , the situation is bit complicated. Figure 15-(c) illustrates the situation, in which  $L_{\Lambda p} = |1, 0\rangle$  in  $z$ -axis is represented as an interfered state of  $|1, \pm 1\rangle$  in  $x$ -axis to make it easy to understand, and the same for  $S_{\Lambda p}$ . Thus,  $S_{\Lambda p}$  and decay-axis are orthogonal as well. Therefore, angular distribution between spin direction and motional direction of proton ( $\theta_{\vec{s}_p - \vec{v}_p}$ ) can be expressed as,

$$N(\phi_{\vec{s}_p - \vec{v}_p}, \theta_{\vec{s}_p - \vec{v}_p}) = \frac{3}{8\pi} \sin^2 \theta_{\vec{s}_p - \vec{v}_p}. \quad (12)$$

Because decay axis should distribute proportionally to  $|Y|^2$ , proton spin is  $\sim$  orthogonal to its motion.

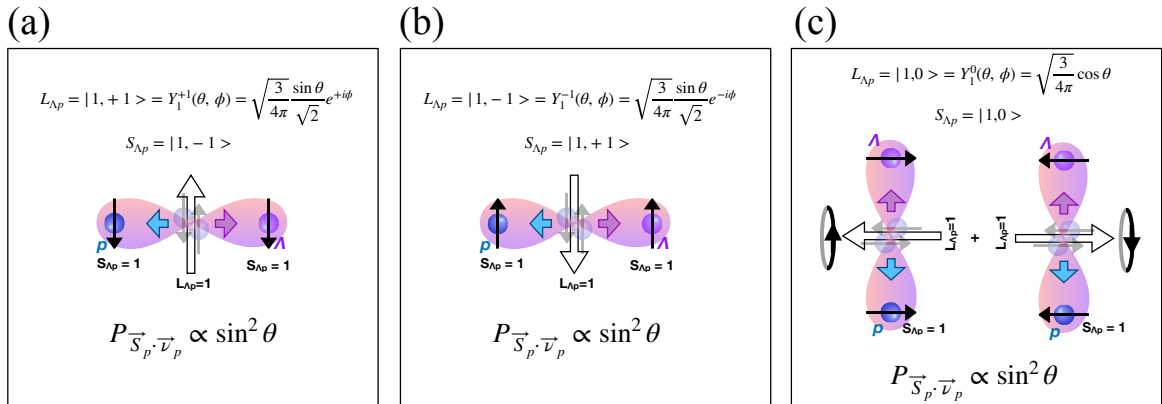


Figure 15: Spin and the decay-axis orientation in  $J^P = 0^-$  with (a)  $S_{\Lambda p} = |1, +1\rangle$ , (b)  $S_{\Lambda p} = |1, -1\rangle$ , and (c)  $S_{\Lambda p} = |1, 0\rangle$ .

In  $J^P = 1^-$ , both  $S_{\Lambda p} = 0$  and 1 are possible to make  $J = 1$ . To derive the ratio between  $S_{\Lambda p} = 0$  and 1, let us consider one specific component of  $P$ -wave  $\bar{K}^0$

absorption on the spin-triplet  $pn$  system,

$$(S_{pn} = |1, +1\rangle) \otimes \bar{K}^0 = \frac{(p\uparrow n\uparrow - n\uparrow p\uparrow)}{\sqrt{2}} \otimes \bar{K}^0, \quad (13)$$

where we set the  $pn$  spin direction as the quantum-axis. All the other  $m$  components should be analogous to this, so it is sufficient. To make  $\Lambda$ ,  $\bar{K}^0$  should be absorbed by the neutron. When  $\bar{K}^0$  couples with  $n\uparrow$  in  $Y_1^m$ ,  $m = 0$  and  $-1$  are possible, and result in  $\Lambda\uparrow$  and  $\Lambda\downarrow$ , with Clebsch-Gordan coefficients of  $-\sqrt{2/3}$  and  $-\sqrt{1/3}$ , respectively. Thus, spin state of  $\Lambda p$ -pair can be written as,

$$\begin{aligned} Y(\theta, \phi)S_{\Lambda p} &= -\sqrt{\frac{2}{3}}\sqrt{\frac{3}{4\pi}}\frac{\sin\theta}{\sqrt{2}}e^{-i\phi}\frac{(p\uparrow\Lambda\downarrow - \Lambda\downarrow p\uparrow)}{\sqrt{2}} - \sqrt{\frac{1}{3}}\sqrt{\frac{3}{4\pi}}\cos\theta\frac{(p\uparrow\Lambda\uparrow - \Lambda\uparrow p\uparrow)}{\sqrt{2}} \\ &= -\sqrt{\frac{1}{3}}\sqrt{\frac{3}{4\pi}}\frac{\sin\theta}{\sqrt{2}}e^{-i\phi}\frac{(p\uparrow\Lambda\downarrow - \Lambda\downarrow p\uparrow) - (p\downarrow\Lambda\uparrow - \Lambda\uparrow p\downarrow)}{\sqrt{2}} \\ &\quad - \sqrt{\frac{1}{3}}\sqrt{\frac{3}{4\pi}}\frac{\sin\theta}{\sqrt{2}}e^{-i\phi}\frac{(p\uparrow\Lambda\downarrow - \Lambda\downarrow p\uparrow) + (p\downarrow\Lambda\uparrow - \Lambda\uparrow p\downarrow)}{\sqrt{2}} \\ &\quad - \sqrt{\frac{1}{3}}\sqrt{\frac{3}{4\pi}}\cos\theta\frac{(p\uparrow\Lambda\uparrow - \Lambda\uparrow p\uparrow)}{\sqrt{2}}, \end{aligned} \quad (14)$$

where  $S_{\Lambda p} = |0, 0\rangle$  in the first term, and  $S_{\Lambda p} = |1, 0\rangle$  and  $|1, +1\rangle$  in the second and third terms, respectively. Therefore,  $\langle S_{\Lambda p} = 0 \rangle : \langle S_{\Lambda p} = 1 \rangle$  is  $1 : 2$ .

Figure 16 shows spin orientation in  $J^P = 1^-$ . In the case of  $S_{\Lambda p} = |0, 0\rangle$  (Fig. 16-(a)), the decay-axis is orthogonal to the quantum-axis, but spin direction is naturally uniform, because the synthetic spin is zero. The decay axis is again orthogonal to the quantum-axis in  $S_{\Lambda p} = |1, 0\rangle$  (Fig. 16-(a)), although spin direction is on the plane orthogonal to the quantum-axis (and uniform in the plane). In  $S_{\Lambda p} = |1, +1\rangle$ , both the decay-axis and spin direction are parallel to the quantum-axis. Consequently, spin and motional direction of proton can be expressed as,

$$N(\phi_{\vec{S}_p - \vec{\nu}_p}, \theta_{\vec{S}_p - \vec{\nu}_p}) = \frac{1}{12\pi} + \left( \frac{1 + 5 \cos^2 \theta_{\vec{S}_p - \vec{\nu}_p}}{16\pi} \right), \quad (15)$$

where the first term corresponds to  $S_{\Lambda p} = 0$  ( $\alpha_{\Lambda p} = -1$ ) and the second term corresponds to  $S_{\Lambda p} = 1$  ( $\alpha_{\Lambda p} + 1$ ). Therefore, proton spin direction is uniform to proton motional direction in  $S_{\Lambda p} = 0$ , and is mostly parallel to the proton motional direction in  $S_{\Lambda p} = 1$ .

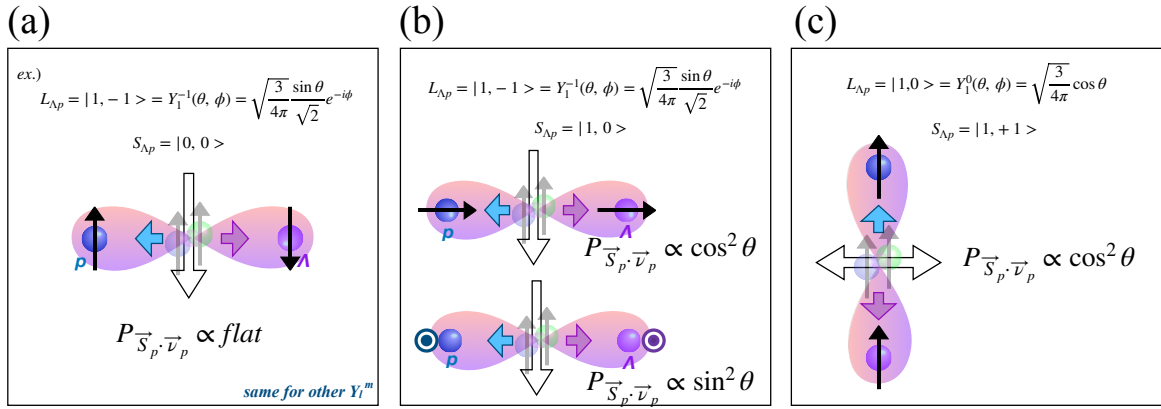


Figure 16: Spin and the decay-axis orientation in  $J^P = 1^-$  with (a)  $S_{\Lambda p} = |0, 0\rangle$ , (b)  $S_{\Lambda p} = |1, 0\rangle$ , and (c)  $S_{\Lambda p} = |1, +1\rangle$ .

## C Expected spectra with neutron detection

Because we are planning to use plastic scintillator as for the polarimeter material, we can use that as for neutron detector having detection efficiency  $\sim 30\%$ . By using that, we can directly detect “ $\bar{K}^0 nn$ ” decay into  $\Lambda n$  and  $\Sigma^- p$  channels. Figure 17 shows expected spectra by detecting  $\Lambda n$ -pair by CDS (missing proton to be identified by the missing-mass). The count-based spectral shape differs from Fig. 9, because the neutron detection efficiency becomes higher at lower momentum. Thus, as shown in Fig. 17-(b), misconceiving background distributed in lower  $m_{\Lambda n}$  region is relatively enhanced by appearance, because the acceptance is uncorrected. A clear signal of “ $\bar{K}^0 nn$ ” is seen again, as it is the case for  $\Lambda p$  detection mode. An advantage of  $\Lambda n$ -pair detection to measure the “ $\bar{K}^0 nn$ ” is acceptance coverage near the lower kinematical limit. By  $\Lambda p$  detection mode, we cannot access this region because proton goes to very forward angle (not covered by CDS). In fact, the inefficient region of this mode deforms the spectra in  $\Lambda p$  detection mode as shown in Fig.9-(a) at just above the lower kinematical limit. Instead, we would obtain reliable production cross section of “ $\bar{K}^0 nn$ ” in  $\Lambda n$  detection mode and it enables us to conduct independent form-factor study also on “ $\bar{K}^0 nn$ ”. This enhanced acceptance region is also inevitable to estimate misconceiving background shape and yield in a reliable manner.

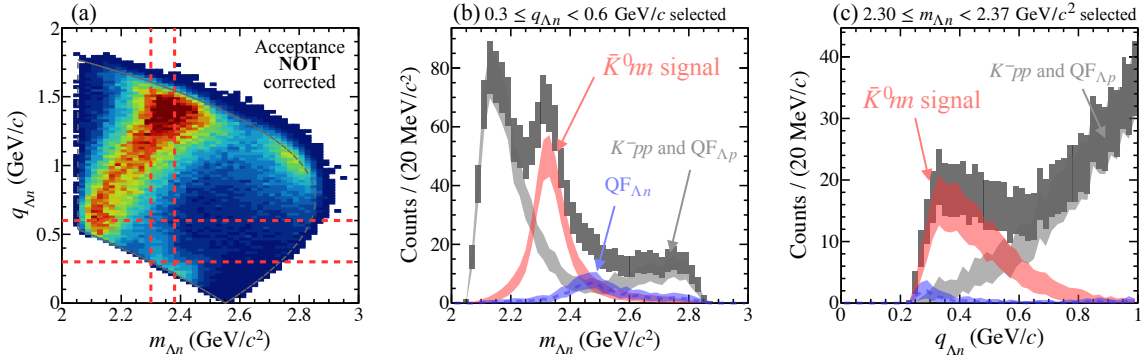


Figure 17: Expected result for the “ $\bar{K}^0 nn$ ” measurement by detecting  $\Lambda n$ -pair in CDS (missing proton to be identified), assuming  $J^P$  of “ $K^- pp$ ” observed in E15 to be  $0^-$ . (a) two-dimensional distribution on the invariant-mass of  $\Lambda n$  ( $m_{\Lambda n}$ ) and momentum transfer to  $\Lambda n$  ( $q_{\Lambda n}$ ). (b) Projection spectrum on the  $m_{\Lambda n}$  axis by selecting  $0.3 \leq q_{\Lambda n} < 0.6$  GeV/c region. (c) Projection spectrum on the  $q_{\Lambda n}$  axis by selecting  $2.3 \leq m_{\Lambda n} < 2.37$  GeV/c region.

We also simulated  $K^- + {}^3\text{He} \rightarrow \Sigma^- pp$  reaction to estimate “ $\bar{K}^0 nn$ ”  $\rightarrow \Sigma^- p$  spectrum. In this reaction, “ $K^- pp$ ” production and  $\text{QF}_{\bar{K}^- \text{abs}}$  going to  $\Lambda p$  channel cannot contribute. Thus, it would be sufficient to consider two processes; “ $\bar{K}^0 nn$ ” production and  $\text{QF}_{\bar{K}^- \text{abs}}$  goes to  $\Sigma^- p$  channels. We assumed these two processes have the same cross section as those of  $\Lambda n$  channel, namely branching ratio of “ $\bar{K}^0 nn$ ”  $\rightarrow \Lambda n$  and  $\Sigma^- p$  are

the same. Figure 18 shows estimated spectrum for  $\Sigma^-p$  detection by its  $\Sigma^-p \rightarrow \pi^-np$  decay chain. Among two protons in the final state,  $p$  from the “ $\bar{K}^0nn$ ” decay is mostly slower than another. Thus, the slower  $p$  is paired with  $\Sigma^-$ . As shown in the figure, “ $\bar{K}^0nn$ ” signal is much better, though the yield is severe. This is because “ $Kpp$ ” and  $QF_{\bar{K}-abs}$  going to  $\Lambda p$  processes, which have larger cross section than “ $\bar{K}^0nn$ ”, cannot to leak in to this channel. It is also advantage for measuring  $q$ -dependence with better S/N ratio as shown in Fig. 18-(c).

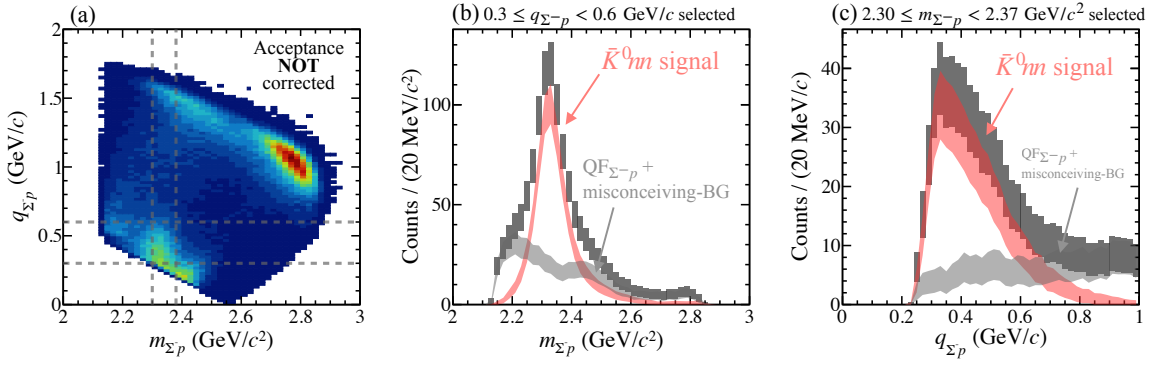


Figure 18: Expected result for the “ $\bar{K}^0nn$ ” measurement by detecting  $\Sigma^-p$ -pair in CDS (missing proton to be identified), assuming  $J^P$  of “ $K^-pp$ ” observed in E15 to be  $0^-$ . (a) two-dimensional distribution on the invariant-mass of  $\Sigma^-p$  ( $m_{\Sigma^-p}$ ) and momentum transfer to  $\Sigma^-p$  ( $q_{\Sigma^-p}$ ). (b) Projection spectrum on the  $m_{\Sigma^-p}$  axis by selecting  $0.3 \leq q_{\Sigma^-p} < 0.6$  GeV/c region. (c) Projection spectrum on the  $q_{\Sigma^-p}$  axis by selecting  $2.3 \leq m_{\Sigma^-p} < 2.37$  GeV/c region.